

Research Paper

Novel *FSIP2* Variants Induce Super-Length Mitochondrial Sheath and Asthenoteratozoospermia in Humans

Mingrong Lv^{1,2,3*}, Dongdong Tang^{1,2,3*}, Hui Yu^{1,6*}, Hao Geng^{1,2,3*}, Yiling Zhou^{7,8*}, Zhongmei Shao^{1,6}, Kuokuo Li^{1,2,3}, Yang Gao^{2,3,4,5}, Senchao Guo^{1,2}, Chuan Xu^{1,2,3}, Qing Tan^{1,9}, Chunyu Liu^{7,8}, Rui Guo^{2,3,4,5}, Huan Wu^{1,2,3}, Zongliu Duan^{1,2,3}, Jingjing Zhang^{1,2,3}, Guanxiong Wang^{1,2,3}, Rong Hua^{2,3,4,5}, Feifei Fu^{1,9}, Kai Wang^{1,2}, Yuping Xu^{1,2,3}, Ping Zhou^{1,2,3}, Zhaolian Wei^{1,2,3}, Feng Zhang^{7,8}✉, Yunxia Cao^{1,2,3}✉ and Xiaojin He^{1,2,3}✉

1. Reproductive Medicine Center, Department of Obstetrics and Gynecology, the First Affiliated Hospital of Anhui Medical University, Hefei 230022, China.
2. NHC Key Laboratory of Study on Abnormal Gametes and Reproductive Tract (Anhui Medical University), Hefei 230032, China.
3. Key Laboratory of Population Health Across Life Cycle (Anhui Medical University), Ministry of Education of the People's Republic of China, Hefei 230032, China.
4. Anhui Province Key Laboratory of Reproductive Health and Genetics, Hefei 230032, China.
5. Biopreservation and Artificial Organs, Anhui Provincial Engineering Research Center, Anhui Medical University, Hefei 230032, China.
6. Department of Obstetrics and Gynecology, Fuyang Hospital of Anhui Medical University, Fuyang 236112, China.
7. Obstetrics and Gynecology Hospital, Institute of Reproduction and Development, Fudan University, Shanghai 200011, China.
8. Shanghai Key Laboratory of Female Reproductive Endocrine Related Diseases, Shanghai 200011, China.
9. Anhui Provincial Human Sperm Bank, the First Affiliated Hospital of Anhui Medical University, Hefei 230022, China.

*These authors contributed equally to this work.

✉ Corresponding authors: **Xiaojin He, MD, PhD**, Professor of Reproductive Medicine Center, Department of Obstetrics and Gynecology, The First Affiliated Hospital of Anhui Medical University, No. 218 Jixi Road, Hefei 230022, China. E-mail: hxj0117@126.com; **Yunxia Cao, MD, PhD**, Professor of Reproductive Medicine Center, Department of Obstetrics and Gynecology, The First Affiliated Hospital of Anhui Medical University, No. 218 Jixi Road, Hefei 230022, China. E-mail: caoyunxia6@126.com; **Feng Zhang, PhD**, Obstetrics and Gynecology Hospital, Institute of Reproduction and Development, Fudan University, Shanghai 200011, China. E-mail: zhangfeng@fudan.edu.cn.

© The author(s). This is an open access article distributed under the terms of the Creative Commons Attribution License (<https://creativecommons.org/licenses/by/4.0/>). See <http://ivyspring.com/terms> for full terms and conditions.

Received: 2022.06.11; Accepted: 2022.11.15; Published: 2023.01.01

Abstract

Asthenoteratozoospermia is one of the major factors for male infertility, whereas the causes of large numbers of cases are still unknown. We identified compound heterozygous variants of *FSIP2* in three unrelated individuals from a cohort of 105 patients with asthenoteratozoospermia by exome sequencing. Deleterious *FSIP2* variations caused severe disassembly of the fibrous sheath and axonemal defects. Intriguingly, spermatozoa in our study manifested “super-length” mitochondrial sheaths, increased levels of the mitochondrial sheath outer membrane protein TOMM20 and decreased mitochondrial ATP consumption. Dislocation or deletion of the annulus and reduction or dislocation of the annulus protein SEPT4 were also observed. While the lengthened mitochondrial sheaths were not presented in men harboring *SEPT4* variants. Furthermore, female partners of two of three men achieved successful pregnancies following intracytoplasmic sperm injection (ICSI). Overall, we presume that *FSIP2* may not only serve as a structural protein of the fibrous sheath but also as an intra-flagellar transporter involving in the axonemal assembly, mitochondrial selection and the termination of mitochondrial sheath extension during spermatogenesis, and ICSI is an effective treatment for individuals with *FSIP2*-associated asthenoteratozoospermia.

Key words: Infertility; asthenoteratozoospermia; mitochondrial sheath; *FSIP2*; ICSI

Introduction

Approximately one-sixth of couples of reproductive age suffer from infertility [1-3]. According to surveys, about 50% of these cases are induced by male factors, defined as male infertility. Sperm defects, including oligozoospermia, asthenozoospermia, and teratozoospermia, are the most common causes of male infertility [4, 5]. Asthenoteratozoospermia, a most common form of male infertility, is characterized

by decreased sperm motility and abnormal sperm morphology and accounts for around 19% of male infertility cases [6, 7].

Teratozoospermia is characterized by the presence of morphologically abnormal sperm with head, neck, and/or flagella defects. Subsequently, morphological deformities cause reduced motility or absent sperm motility. The abnormal sperm flagella

presents with absent, short, bent, coiled, or irregular flagella [8, 9]. Human sperm flagellum contain three parts based on the unique accessory structures surrounding the axoneme: mid-piece, principal piece, and end-piece [9]. The axoneme, an evolutionarily conserved motile cilia and sperm flagellum structure, comprises nine peripheral double-microtubules (DMT) enveloping two central pairs (CP), termed the "9+2" structure, throughout the flagellum [10]. In the mid-piece, the axoneme is wrapped by outer dense fibers (ODFs) and a mitochondrial sheath (MS) that is replaced with the fibrous sheath (FS) in the principal piece, with no peri-axonemal structure in the end piece [9, 11]. Defects in the axoneme, peri-axoneme, protein transport, or centriole assembly can lead to defective sperm flagella, resulting in asthenoteratozoospermia. For example, variations in several dynein axonemal heavy chain (DNAH) family member genes [12-17] and cilia and flagella associated protein (CFAP) genes can cause various structural abnormalities in the axoneme [18-21]. Moreover, variations in *TTC21A* (MIM: 618429), *TTC29* (MIM: 618735), and *CFAP69* (MIM: 617949) can severely disrupt flagellar axoneme assembly through the intra-flagellar transport (IFT) and intra-manchette transport (IMT) pathways during spermiogenesis [22-24]. In addition, bi-allelic variations in *DZIP1* (MIM: 608671) and *CEP135* can cause severe defects due to abnormal centriole assembly. Owing to high phenotypic variability, the genetic causes of asthenoteratozoospermia remain largely unknown [25, 26].

The fibrous sheath (FS) is the first accessory structure formed after axoneme initiation during sperm tail development. In mature sperms, the FS is composed of longitudinal columns connected by transverse ribs [27]. The A-kinase anchoring proteins (AKAPs), namely, AKAP3, AKAP4, and AKAP14, are the major components of the FS. Variations in *AKAP3* and *AKAP4* cause dysplasia of the fibrous sheath (DFS) [28, 29]. Fibrous sheath-interacting protein 2 (*FSIP2*) localizes to the FS and directly interacts with AKAP4 [30]. Variations in *FSIP2* lead to loss of components of central microtubules, including CP, and complete defects in the axoneme, resulting in the multiple morphological abnormalities of the sperm flagella (MMAF) phenotype presenting with absent, short, coiled flagella [31-34]. Although more than 15 proteins have been found to be involved in the FS [9], how they assemble this unique cytoskeletal structure remains unclear.

The mitochondrial sheath (MS) is arranged helically over nine ODFs and an axoneme in the mid-piece of the sperm flagellum. In humans, formation of the MS needs the redistribution of

mitochondria from a broad cytoplasmic distribution to the sperm tail, with the last 72–80 elongated mitochondria forming a helix of approximately 10–12 gyres [35], with two mitochondria per gyrus. The number of gyres and the length of the MS are strictly regulated during late spermatogenesis [27, 36]. In mice, previous studies found that the mitochondria were accumulated in the midpiece regions of *Cfap157* null sperm [37]. ARMC12 interacted with mitochondrial proteins VDAC2, VDAC3, and MIC60 as well as TBC1D21 and GK2, regulating the mitochondrial interlocking step [38]. Similarly, deficiency of TBC1D21, a loose and inordinate mitochondrial sheath assembled a hairpin like sperm flagella, losing interacting with ACTB, TPM3, SPATA19, and VDAC3 [39]. In mitochondrial fission factor (*Mff*) mutant mice, mitochondrial sheaths of elongating spermatids and spermatozoa are disjointed, swollen mitochondria arranged loosely [40]. *Glycerol kinase 2* (*Gk2*)-deficiency sperm showed abnormal localization of crescent-like mitochondria [39, 41]. *Fsip1*^{-/-} sperm revealed abnormal accumulation of mitochondria [42]. In humans, abnormalities in spermatozoa, including shorter mid-pieces with fewer mitochondrial gyres, abnormal mitochondrial assembly, and structural defects in mitochondrial membranes, have been associated with asthenozoospermia [43-45]. Moreover, except for specific flagellum defects present in the MMAF phenotype, variations in *CFAP65* (MIM: 614270), *CFAP58* (MIM: 619129), *EIF4G1* (MIM: 600495), and *DNH1* (MIM: 617277) also cause sperm MS malformations [19, 46-48]. However, the mechanisms underlying these defects during spermatogenesis are not clearly understood.

In this study, we used whole-exome sequencing (WES) to identify compound heterozygous variations in three unrelated subjects from a cohort of 105 individuals with asthenoteratozoospermia. *FSIP2* variations led to significant reductions in *FSIP2* mRNA and protein levels, resulting in the disruption or loss of FS. Subsequently, *FSIP2* deficiency was considered the leading cause of axoneme disorganization. Additionally, we found that *FSIP2* deficiency induced the elongation of the mitochondrial sheath and eliminated the annulus ring. The absence of annulus ring was not associated with the super-length MS in sperm from subjects harboring *SEPT4* variants. Furthermore, the partners of two patients achieved successful pregnancy outcomes following intracytoplasmic sperm injection (ICSI). Thus, we speculate that *FSIP2* may serve as both a structural protein of the fibrous sheath and a component of intra-flagellar transporter complex participating in the assembly of flagellum and MS during spermatogenesis. Lastly, our study also provided clinical evidence that ICSI is

an effective treatment for individuals with *FSIP2*-associated asthenoteratozoospermia.

Materials and Methods

Study participants

We enrolled 105 infertile men with asthenoteratozoospermia from the reproductive medicine center of the First Affiliated Hospital of Anhui Medical University. Detailed clinical manifestations of primary ciliary dyskinesia-related symptoms (i.e. sinusitis, pneumonia, and bronchitis) were reviewed and excluded. Clinical examination revealed normal male testicle size, external genitalia, hormone levels, and secondary sexual characteristics. Each individual had the chromosomal karyotype 46, XY. No Y chromosome microdeletions were identified. The present study was approved by the Ethics Committee of Anhui Medical University. All participants involved in this study signed the informed consents before collecting peripheral blood or semen samples.

Whole-exome sequencing (WES)

Peripheral whole blood samples were collected from the asthenoteratozoospermia-affected individuals, and genomic DNA extraction and exome enrichment were performed. Briefly, qualified genomic DNA samples were sequenced on the Illumina HiSeq X-TEN platform. Raw data generated from each sample were aligned against the human reference genome (UCSC Genome Browser hg19) using the Burrows-Wheeler Aligner (BWA) algorithm after removing low-quality reads. All genomic variations, including single nucleotide variations and InDels, were annotated and filtered. Variant screening was conducted as previously described [49]. ANNOVAR software (Version: 2020-06-08) was used for functional annotation using information from various databases and bioinformatics tools, including OMIM, Gene Ontology, SIFT, PolyPhen-2, 1000 Genomes Project, and gnomAD [50]. Pathogenic variants in genes, testis-specific expressed or biased expression in testis, were selected as candidates. In humans, testis-specific expression or biased expression in testis was defined as an average expression value of ≥ 5 reads per kilobase per million map reads in the testis and more than 2-folds of the average expression value in other tissues based on the GTEx. Candidate variants were validated using Sanger sequencing. The primers used to validate *FSIP2* variants are listed in Table S1.

Sperm motility, morphology and viability measurements

Parameters of semen from healthy and infertile men were analyzed using computer-assisted sperm

analysis based on WHO guidelines (6th Edition) during routine biological examination [51]. Briefly, semen samples were collected through masturbation after 3–7 days of sexual abstinence and examined after liquefaction at 37 °C for 30 min. Each individual's semen parameters were measured at least three times. H&E and Papanicolaou staining was used to analyze sperm morphology. Briefly, sperm samples were fixed with 4% paraformaldehyde, dehydrated, and then stained with H&E and Papanicolaou. At least 200 spermatozoa from each sample were assessed, based on WHO guidelines, to determine the percentage of morphologically abnormal spermatozoa. Each flagellum was classified into a morphological category based on the main flagellar abnormality.

Regarding to the sperm vitality test, we used eosin staining partly based on 6th WHO guidelines. Briefly, mix a 50 μ l aliquot of semen sample with an equal volume of eosin-suspension in a test tube, and wait for 30 seconds. Make a smear on a glass slide and examine the slide with bright field optics at $\times 1000$ magnification and oil immersion. Evaluate at least 200 spermatozoa, to achieve an acceptably low sampling error. Spermatozoa with red or dark pink heads are considered dead, whereas spermatozoa with white heads are considered alive.

Scanning electron microscopy (SEM) and transmission electron microscopy (TEM) analyses

Fresh semen samples from normal controls and men carrying *FSIP2* variants were washed three times with 1 \times phosphate-buffered saline (PBS), centrifuged at 2500 rpm for 10 min and then fixed with 2.5% glutaraldehyde (pH 6.9) for 2 h at 4 °C.

For SEM, fixed spermatozoa were progressively dehydrated using increasing concentrations of ethanol (30%, 50%, 70%, 80%, 90%, and 100%) and then dried in a K850 CO₂ critical point dryer (Quorum Technologies, Lewes, UK). The specimens were then coated with metal particles using a Cressington 108 Auto carbon coater (Cressington Scientific Instruments Ltd, Watford, UK) and analyzed under a GeminiSEM 300 scanning electron microscope (ZEISS, Oberkochen, Germany).

For TEM, fixed spermatozoa were post-fixed with 1% osmium tetroxide for 2 h at 4 °C, dyed with 2% uranium acetate for 2 h, and dehydrated in a graded series of ethanol (50%, 70%, 90%, and 100%) and 100% acetone. The fixed spermatozoa were then embedded in EPON 812 epoxy resin. Finally, the embedded spermatozoa were sliced into ultrathin sections (100nm thick), stained with lead citrate, and observed under a Talos L120C G2 transmission electron microscope (Thermo Fisher Scientific,

Waltham, MA, USA).

Real time PCR analysis

Sperm samples were collected from three fertile men and three patients carrying *FSIP2* variants. At least three semen samples from each patient were collected over 3 months through masturbation after 3-7 days of sexual abstinence. Total RNA was extracted from the sperm samples using TRIzol reagent (Invitrogen, Waltham, MA, USA). Approximately 1 µg of the obtained RNA was converted into cDNA using SuperScript III Reverse Transcriptase and oligo (dT) primers (TaKaRa Bio, Kusatsu, Shiga, Japan). The cDNA was used as a template in subsequent PCR amplification with transcript-specific primers (Table S1). Quantitative real-time polymerase chain reaction (RT-qPCR) was performed, with β-actin as an internal control. Data were analyzed using the $2^{-\Delta\Delta C_t}$ method.

Immunofluorescence analysis

Immunofluorescence (IF) analysis was performed using sperm cells from healthy controls and patients carrying *FSIP2* variants. The procedures, including sample fixation, smear preparation, antigen blocking, and antibody incubation, were performed as previously described [25]. The following were used as primary antibodies: rabbit polyclonal anti-SEPT4 (Affinity, DF13393, 1:200), rabbit polyclonal anti-TOMM20 (Proteintech, 11802-1-AP, 1:400), rabbit polyclonal anti-AKAP4 (Sigma-Aldrich, HPA020046, 1:200), rabbit polyclonal anti-SPAG6 (Sigma-Aldrich, HPA038440, 1:200), rabbit polyclonal anti-FSIP2 (Sigma-Aldrich, HPA036139, 1:50), mouse polyclonal anti-TOMM20 (Proteintech, 66777-1-Ig, 1:200), rabbit polyclonal anti-DNAI2 (Proteintech, 17533-1-AP, 1:200), rabbit polyclonal anti-IFT88 (Proteintech, 13967-1-AP, 1:200), rabbit-polyclonal anti-IFT74 (Sigma Aldrich, HPA020247, 1:200), rabbit-polyclonal anti-IFT20 (Abcepta, Cat# AP5133C, 1:200), and mouse monoclonal anti-acetylated-tubulin (Sigma-Aldrich, T6793, 1:200). After washing with PBS, slides were incubated for 1 h at 37 °C with highly cross-adsorbed secondary antibodies: Alexa Fluor 488 anti-mouse IgG (Yeasen Biotechnology, 34106ES60, 1:500) and Alexa Fluor 594 anti-rabbit IgG antibodies (Jackson ImmunoResearch Inc., 111-585-003, 1:500). The nuclei were then labeled with Hoechst nuclear stain (Thermo Fisher Scientific Inc., 62,249, 1:1000) and incubated at 37 °C for 5 min. Images were captured using the LSM 800 confocal microscope (Carl Zeiss AG).

Western blot (WB) analysis

Proteins were isolated from spermatozoa samples using RIPA lysis buffer (Beyotime

Biotechnology) and used for western blot analysis. The lysates were separated on a 10% polyacrylamide gel using sodium dodecyl sulfate-polyacrylamide gel electrophoresis and transferred onto polyvinylidene fluoride membranes. To block non-specific binding to the membranes, the blots were blocked with 5% non-fat milk in Tris-buffered saline containing 0.1% Tween-20 for 1 h at 25 °C. The blots were then incubated with shaking overnight at 4 °C with primary antibodies diluted in TBST. Rabbit polyclonal SEPT4 (1:1000), rabbit polyclonal anti-TOMM20 (1:1000), rabbit polyclonal anti-AKAP4 (1:1000), rabbit polyclonal anti-SPAG6 (1:1000), rabbit polyclonal anti-DNAI2 (1: 1000), rabbit polyclonal anti-IFT88 (1:1000), rabbit polyclonal anti-IFT74 (1:1000), rabbit polyclonal anti-IFT20 (1:1000), and mouse polyclonal anti-β-actin were used. The blots were subsequently washed in TBST and incubated at 25 °C for 1 h with 1:5000 dilutions of HRP-conjugated secondary antibody. Enhanced chemiluminescence (Biosharp, BL520A) was used to visualize target proteins, and β-actin was used as the loading control.

Measurement of ATP content

The amount of spermatozoa ATP was examined using CellTiter-Glo luminescent cell viability assay Kit (Promega, USA) according to the manufacturer's instructions. After 30 min incubation to allow for sperm liquefaction (at 37 °C in 5% CO₂ atmosphere), we immediately measured ATP contents (time point 0) in SpectraMax iD3 (Molecular Devices, US). A second measure was similarly performed after sperm incubation for another 1 h. All measures were performed in triplicated for each semen sample. Three semen samples were collected three times from each patient. ATP content was calculated using an ATP standard curve (dilutions of ATP in medium from 10 µM to 10 nM).

Assessment of sperm mitochondrial membrane potential

Mitochondrial membrane potential was assessed using JC-1 assay kit according to the instructions described previously [52]. JC-1-stained sperm samples were analyzed by flow cytometry (BD FACSVerser™ Flow Cytometer (BD Biosciences, USA)) collecting 50000 cells. JC-1 exists inside the mitochondria in the J-aggregates form and emits red fluorescence (PI channel), representing high mitochondrial membrane potential (MMP). Whereas, it remains in the monomer form and emits green fluorescence (FITC channel), representing in a low MMP state.

Statistical analysis

Data obtained from RT-qPCR were analyzed using GraphPad Prism (GraphPad Software, San

Diego, CA, USA), and fold-change in RNA expression was calculated using the $2^{-\Delta\Delta Ct}$ method. Morphological data from two participants were evaluated and then statistically rated, with statistical significance set at $p < 0.05$.

Results

Identification of deleterious *FSIP2* variants in three individuals with asthenoteratozoospermia

In this study, WES and bioinformatics analyses were performed according to a previously described protocol [19] and three compound heterozygous *FSIP2* variants (NM_173651.4) were identified in three unrelated subjects. All identified variants were verified using Sanger sequencing. Compound heterozygous c.8104dup (p.L2702Pfs*44) and c.4574C>A (p.S1525*) in family 1 (P1), compound heterozygous c.8038dup (p.T2680Nfs*9) and c.9234dup (p.L3079Tfs*6) in family 2 (P2), and compound heterozygous c.10247dup (p.3417Gfs*12) and c.9043G>A (p.E3015K) in family 3 (P3) were inherited from heterozygous parents, consistent with an autosomal recessive mode of inheritance (Fig. 1A). *FSIP2* protein is one of the main component of the flagella FS. It contains three *FSIP2* domains and a coiled-coil domain. The frameshift variants (M1-M5) identified in this study presumably result in premature termination codons and truncated proteins, suggesting their strong deleterious effects (Fig. 1B, Table 1). The remaining missense variant was highly conserved across species and predicted to be damaging (Fig. 1B, Table 1). Notably, analysis of the prevalence of these variants in the 1000 Genomes and gnomAD databases revealed that the variants were either extremely rare or absent in the general population (Table 1). Therefore, we hypothesized that *FSIP2* variants identified here may be responsible for the observed infertility phenotypes.

FSIP2 variants are associated with the sperm super-length mitochondrial sheaths and thicker mid-pieces

Sperm parameters were examined in the clinical laboratories during routine biological examinations of patients, in accordance with the 6th World Health Organization (WHO) guidelines [51]. Normal semen volumes and sperm concentrations were observed in patients carrying *FSIP2* variants; however, sperm motility and progressive motility were lower (Table 2). The morphology of sperm cells from patients carrying *FSIP2* variants was assessed using H&E and Papanicolaou staining (Fig. 2A), and morphologically abnormal spermatozoa were evaluated according to

WHO guidelines. Sperm morphological analysis showed that most of spermatozoa displayed with elongated mid-pieces connected to the short or thin principal pieces with or without dysplastic fibrous sheath surrounding (Fig. 2A and Table 2). Approximately, one third of sperm necks were thickened by encapsulated in excess residual cytoplasm (ERC) (Table 2). Meanwhile, the defective sperm head mainly presented with amorphous head and vacuolated acrosome (Table 2). SEM confirmed the phenotypes observed above in two cases. Intriguingly, SEM revealed thicker necks and longer mitochondrial sheaths in the mid-pieces and dysplastic sperm FS in the principal pieces in individuals carrying *FSIP2* variants compared with normal controls (Fig. 2B). We also investigated the sperm flagellar ultrastructure in individuals carrying *FSIP2* variants using TEM. Longitudinal sections of sperm flagella observed using TEM revealed that, compared with normal controls, the MS was more than twice as long in individuals carrying *FSIP2* variants. Additionally, compared with the regularly arranged mitochondrial sheath and the fibrous sheath connected by the annulus observed in normal sperm, sperm in individuals carrying *FSIP2* variants had no annulus and exhibited severe FS dysplasia (Fig. 2C and 2D). These findings suggest that the *FSIP2* variants not only affect the assembly of the FS but also affect the elongation of the mitochondrial sheath.

Severe disorganization of axonemal and fibrous sheath structures in individuals carrying *FSIP2* variants

TEM was used to assess the effect of *FSIP2* compound heterozygous variations on the sperm flagellar ultrastructure. Compared with fertile controls, a variety of ultrastructural defects were observed in the mid-piece of spermatozoa from patients with *FSIP2* deficiency. We found integrated and regularly arranged DMT and ODF in patients. The CP was missing from the mid-pieces of 24% of flagella from P1 and 21% of flagella from P2. In addition, multiple FS with disassembled DMTs and ODFs, multiple bare axonemes, or some doublets of microtubules (DMT) scattered throughout excess residual cytoplasm were also observed surrounding the mid-piece, presenting with thick neck, which accounted for about 27% in P1 and 30% in P2. The remaining cross-sections had highly disorganized mid-pieces (19% and 25%) (Fig. 3A and 3C). As shown in Fig. 3B, in the normal principal piece, the axoneme is surrounded by seven ODFs and flanked by an FS composed of two longitudinal columns connected by circumferential ribs (ODFs 3 and 8 are replaced by two longitudinal columns). Analysis of individuals

with *FSIP2* deficiency showed that 36% and 43% of the cross-sections had disordered FS surrounding the axoneme; 34% and 31% of the analyzed cross-sections lacked axonemes and regularly arranged ODFs, while others exhibited disorganized axonemes and ODFs.

Additionally, nine ODFs were observed around the axoneme in the cross-sections of some principal pieces, suggesting that the 3rd and 8th ODF were not replaced by longitudinal columns (Fig. 3B and 3D).

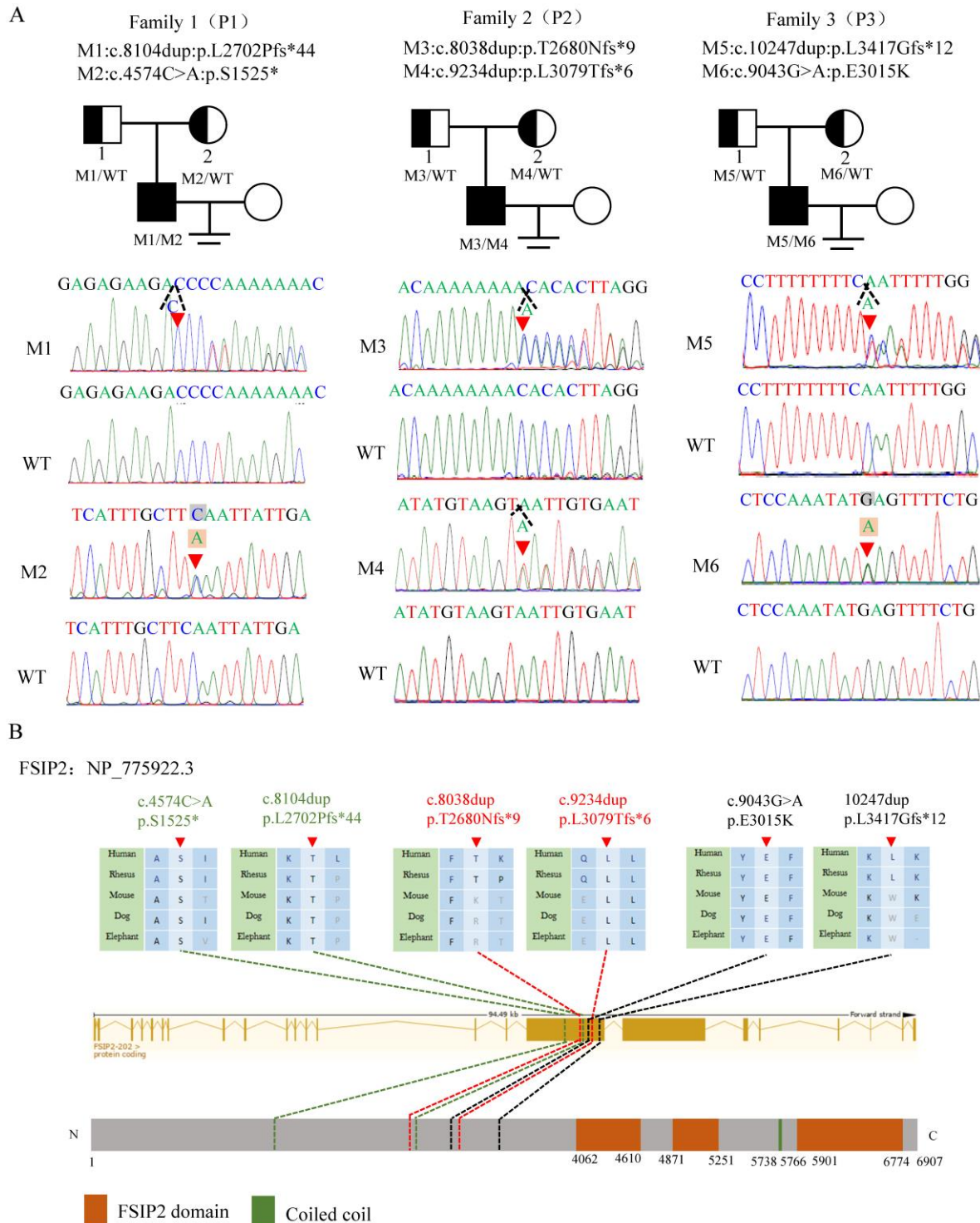


Figure 1. Compound heterozygous variants of *FSIP2* in three families with MMAF-affected asthenoteratozoospermia. (A) Novel *FSIP2* variants (M-M6) were identified in three subjects with MMAF (P1, P2 and P3). The heterozygous parental carriers of all *FSIP2* variants are shown. Arrows (red) show the positions of novel *FSIP2* variants identified in the present study. The triangle dotted lines (black) show positions of duplicated bases and squares stand for the bases (grey) were replaced by another ones (light orange). **(B)** Schematic representation of exons and protein product of *FSIP2* gene. Arrows (red) and dotted lines show (green, red and black) the positions of novel *FSIP2* variants identified in the present study. Sequence alignments show conservation of the affected amino acid across different species. Orange squares stand for the *FSIP2* domains and green square stands for the typical protein-folding motif called coiled-coil (CC) domain according to the NCBI browser. WT, wild type, M, mutation, P, patient.

Table 1. Bi-allelic Variants of *FSIP2* Variants Identified in Chinese Men

<i>FSIP2</i> Variant	P1		P2		P3	
cDNA alteration	c.8104dup	c.4574C>A	c.8038dup	c.9234dup	c.10247dup	c.9043G>A
Variant allele	Het	Het	Het	Het	Het	Het
Protein alteration	p.L2702Pfs*44	p.S1525*	p.T2680Nfs*9	p.L3079Tfs*6	p.E3417Gfs*12	p.E3015K
Variant type	frameshift	stop-gain	frameshift	frameshift	frameshift	Missense
Allele Frequency in Human Population						
1000 Genomes						
gnomAD	NA ^a	NA ^a	9.1×10 ⁻⁵	NA ^a	7.0×10 ⁻⁵	NA ^a
gnomAD-EAS	NA ^a	NA ^a	0	NA ^a	0	NA ^a
Function Prediction						
SIFT	NA ^b	NA ^b	NA ^b	NA ^b	NA ^b	D
PolyPhen-2	NA ^b	NA ^b	NA ^b	NA ^b	NA ^b	NA ^b
Mutation Taster	NA ^b	NA ^b	NA ^b	NA ^b	NA ^b	D
CADD	NA ^b	35.0	NA ^b	NA ^b	NA ^b	22.3

The accession number of human *FSIP2* is GenBank: NM_173651.4.

Full-length *FSIP2* has 6907 amino acids.

Abbreviations are as follows: Het, heterozygous; NA^a, not available; NA^b, not assessed; D, deleterious.

Table 2. Semen Characteristics and Sperm Morphology in Chinese Men with Bi-allelic *FSIP2* Mutations

Subject	P1	P2	P3	Reference Limits
Age	30	27	29	
Semen Parameter				
Semen volume (mL)	1.0	3.7	2.075	>1.5
Semen concentration (10 ⁶ /mL)	47.08	63.1	57.325	>15.0
Motility (%)	5.99	25	13	>40.0
Progressive motility (%)	3.39	5.4	4.45	>32.0
Sperm Morphology				
Normal flagella (%)	0	0	/	>23.0
Absent flagella (%)	0.7	0	/	<5.0
Short flagella (%)	41.3	32.7	/	<1.0
Coiled flagella (%)	5.8	3.7	/	<17.0
Angulation (%)	2.4	1.5	/	<13.0
Thin (%)	50.0	62.1	/	
Mid-piece Morphology				
Insert (%)	0.5	1.5	/	
Angulation (%)	0.9	1.5	/	
Lengthened (%)	92.9	100		
ERC (%)	32.7	33.8		
Head Morphology				
Normal (%)	21.3	26.5	/	
Amorphous head (%)	71.3	66.2	/	
Vacuolated (%)	28.2	21.6	/	
Small acrosomes (%)	5.0	1.0	/	

FSIP2 is exclusively expressed in human and mouse testis [31]. To understand the pathogenicity associated with *FSIP2* variants, we examined the expression and localization of *FSIP2* in sperm cells collected from normal controls and patients carrying *FSIP2* variants using RT-qPCR and immunofluorescence. RT-qPCR results showed that *FSIP2* mRNA expression was significantly lower in patients carrying *FSIP2* variants than in normal controls (Fig. 3E). As shown in Fig. 3F, the *FSIP2* staining signal was strong in the flagella of control sperm cells from fertile individuals, but the corresponding signal was almost absent in spermatozoa of individuals carrying *FSIP2* variants. The *FSIP2* antibody epitope is located after the mutation for P1 and P2. A possible truncated protein is therefore not recognized by the antibody, or possible due to nonsense-mediated mRNA decay triggered by premature translation termination. Collectively, these variations had a negative effect on

FSIP2 expression, potentially disrupting sperm flagellar development and leading to the asthenoteratozoospermia phenotype.

***FSIP2* deficiency is associated with increased mitochondrial protein, decreased ATP consumption and altered distribution of annulus components**

Morphological and ultrastructural analyses of spermatozoa from individuals carrying *FSIP2* variants indicated that *FSIP2* may play an essential role in mitochondrial sheath assembly and sperm flagellar formation. To investigate the effect of *FSIP2* variations on the mitochondrial sheath assembly state, we evaluated expression levels and localization of the mitochondrial outer membrane protein TOMM20. In normal sperm, TOMM20 staining signals were concentrated outside the mid-piece, the length of which were about 5 μm , approximately the same length as the sperm head. Conversely, the corresponding staining signals showed that the length of mid-pieces were $13.04 \pm 3.71 \mu\text{m}$ in sperm from P1 and $14.20 \pm 3.99 \mu\text{m}$ in sperm from P2, 2-3 times of that in control sperm (Fig. 4A, B and C). To determine whether the lengthened mitochondrial sheath was associated with *FSIP2* variants, as opposed to being a hallmark of the MMAF phenotype, we also performed TOMM20 immunofluorescence assays on sperm cells from individuals with *FSIP2* variants (A011) reported previously [32] and subjects with MMAF who carried variants in *DNAH10* and *TTC21A* genes. The length of TOMM20 staining signal in sperm from A011 ($8.43 \pm 4.77 \mu\text{m}$) was also increased significantly, about twice that of normal sperm (Fig. 4A, B and C). While, TOMM20 staining signals of sperm cells from individuals harboring *DNAH10* and *TTC21A* variants were comparable with those observed in fertile controls (Fig. S1). Consistently, WB staining showed that levels of TOMM20 protein were higher 1-2 times in P1 and P2 than those in normal controls (Fig. 4D

and E). In addition, ac-tubulin immunofluorescence staining showed that axonemal malformations, including disruption of the DMT structure and the growth of multiple flagella from the neck, which then

surrounded the mitochondria, were observed in many spermatozoa in individuals carrying *FSIP2* variants (Fig. 4A). Overall, these findings were in accordance with the SEM and TEM observations.

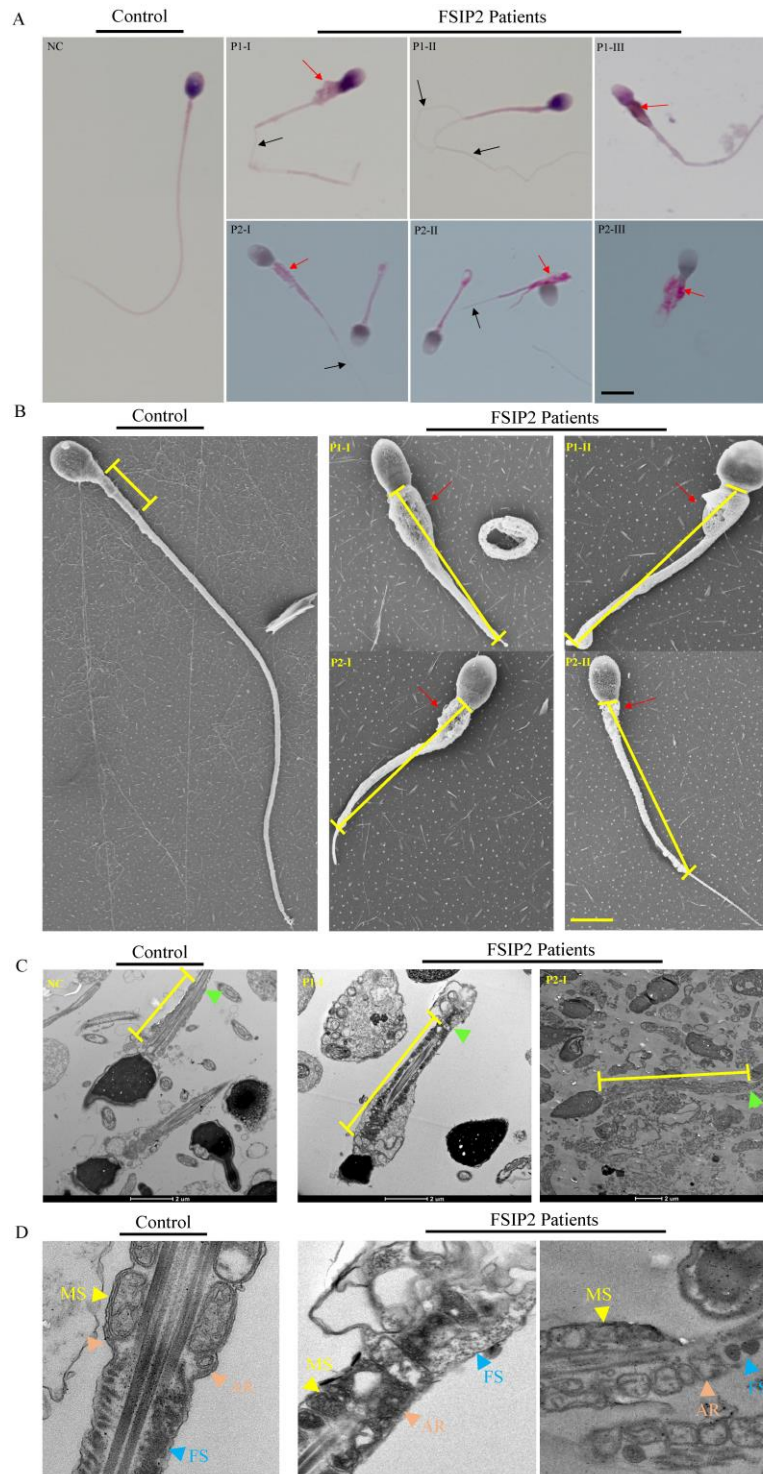


Figure 2. Morphology and ultrastructure analysis of spermatozoa in the fertile males and men harboring *FSIP2* variants. (A) Morphological sperm defects analyzed through light microscopy (100 \times , oil objective, scale bar: 10 μ m) by H&E (NC and P1) and Papanicolaou (P2) staining. Spermatozoa from the fertile control showed normal long and smooth flagella, whereas abnormal thick neck (red arrow), multiple thin flagella (black arrow), short, coiled flagella, flagella of angulation and irregular caliber could be obviously observed in the spermatozoa of *FSIP2*-deficient men. (B) SEM analysis of sperm morphology from a normal control and *FSIP2*-deficient subjects. Most spermatozoa from men harboring *FSIP2* variants presented thickened neck (red arrow) and lengthened mid-piece (yellow line). Scale bar: 5 μ m. (C and D) Electron micrographs of longitudinal sections of sperm flagellar mid-piece of a control individual and men harboring *FSIP2* variants. The normal sperm mid-piece had a regularly arranged MS (yellow arrows) with the length of about 5 μ m adjacent to the FS connected by annulus ring (brown arrows). While, the extension of mitochondrial sheath in *FSIP2*-deficient subjects showed a significantly lengthened with destroyed or absent fibrous sheath (blue arrows). MS, mitochondrial sheath, FS, fibrous sheath, P1, patient 1, P2, patient 2, Scale bars: 2 μ m and 1 μ m.

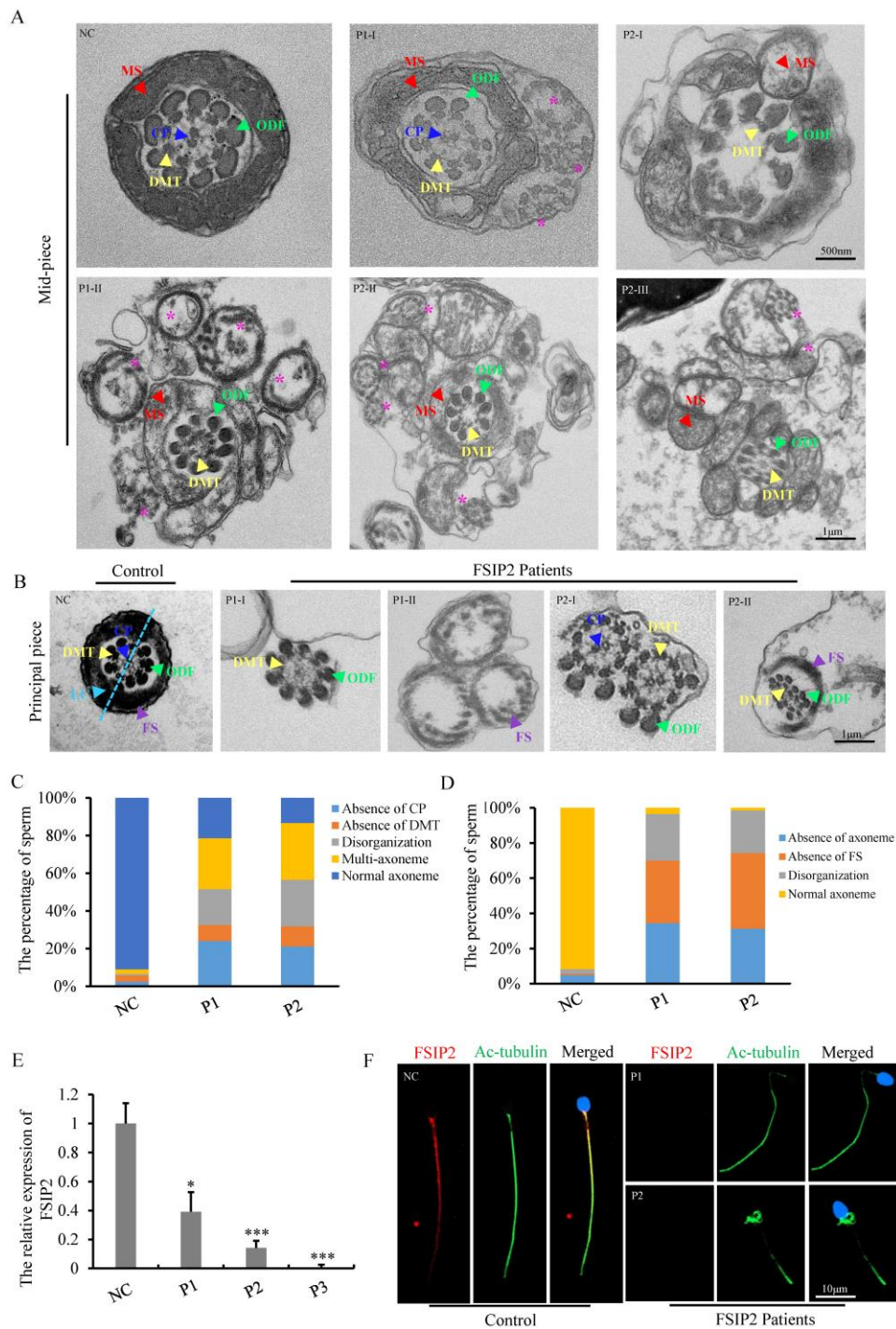


Figure 3. FSIP2 deficiency associated with sperm axoneme malformations and central pair absence. (A) Transmission electron microscopy (TEM) of analysis of sperm mid-piece ultra-structure in *FSIP2*-deficient human subjects. Cross section of sperm from a normal subject presented the typical normal “9+2” microtubule structure with CP (blue arrow), DMT (yellow arrow), MS (red arrow) and arrangement of ODF (green arrow). Compared with the control subject, mid-piece with absence of CP, or surrounded by multiple axoneme (pink stars) without FS or/and empty FS or increased mitochondria can be observed in the subjects with *FSIP2* variants, CP, central pair, DMT, doublets of microtubules, MS, mitochondrial sheath, ODF, outer dense fibers, Scale bars: 1 μ m. **(B)** TEM of analysis of sperm principal piece ultra-structure in *FSIP2*-deficient subjects. In the control subject, the axoneme is surrounded by seven ODFs and by the FS composed of two longitudinal columns (LC, marked by light blue dotted line and arrow) connected by circumferential ribs. Cross-sections of sperm flagellum from *FSIP2* deficient subjects, the FS is absent (P1-I and P2-I), dysplastic without LC (P2-II) or dramatically disorganized (P1-II and P2-II). Various axonemal anomalies can be observed including the lack of axoneme or CP, or complete axonemal disorganization. Additionally, alterations of ODFs is also seen with missing or fully disorganized ODFs. Scale bars: 1 μ m. **(C and D)** Quantification of different categories of flagellar mid-piece and principal piece ultrastructural defects. Total cross-section numbers for quantification in the control subject and men harboring *FSIP2* variants (P1 and P2) were 121, 178 and 113, respectively. Cross-sectional defects were classified into four categories: absence of CP (24.2% & 21.2% for subjects P1 and P2), absence of DMT (8.4% & 10.6%), disorganization (19.1% & 24.8%) and multi-axoneme (27% & 30.1%). Total cross-section numbers for quantification in the control subject and men harboring *FSIP2* variants (P1 and P2) were 120, 87 and 70, respectively. Cross-sectional defects were classified into three categories: absence of axoneme (34.5% & 31.4%), absence of FS (35.6% & 41.9%) and disorganization (26.4% & 24.3%). **(E)** The relative mRNA expression levels of *FSIP2* in sperm from *FSIP2*-deficient subjects and three control subjects. The *FSIP2* mRNA level of *FSIP2*-deficient subjects was significantly reduced compared with that in the controls. * $P < 0.05$, *** $P < 0.001$. **(F)** *FSIP2* immunofluorescence assays of human sperm. Immunofluorescence staining reveals the absence of specific staining of *FSIP2* in sperm flagella from patients with *FSIP2* compound heterozygous variants. Anti-ac-tubulin (green) marked the sperm flagella. The nuclei of spermatozoa were Hoechst-labeled (blue). Scale bars: 10 μ m.

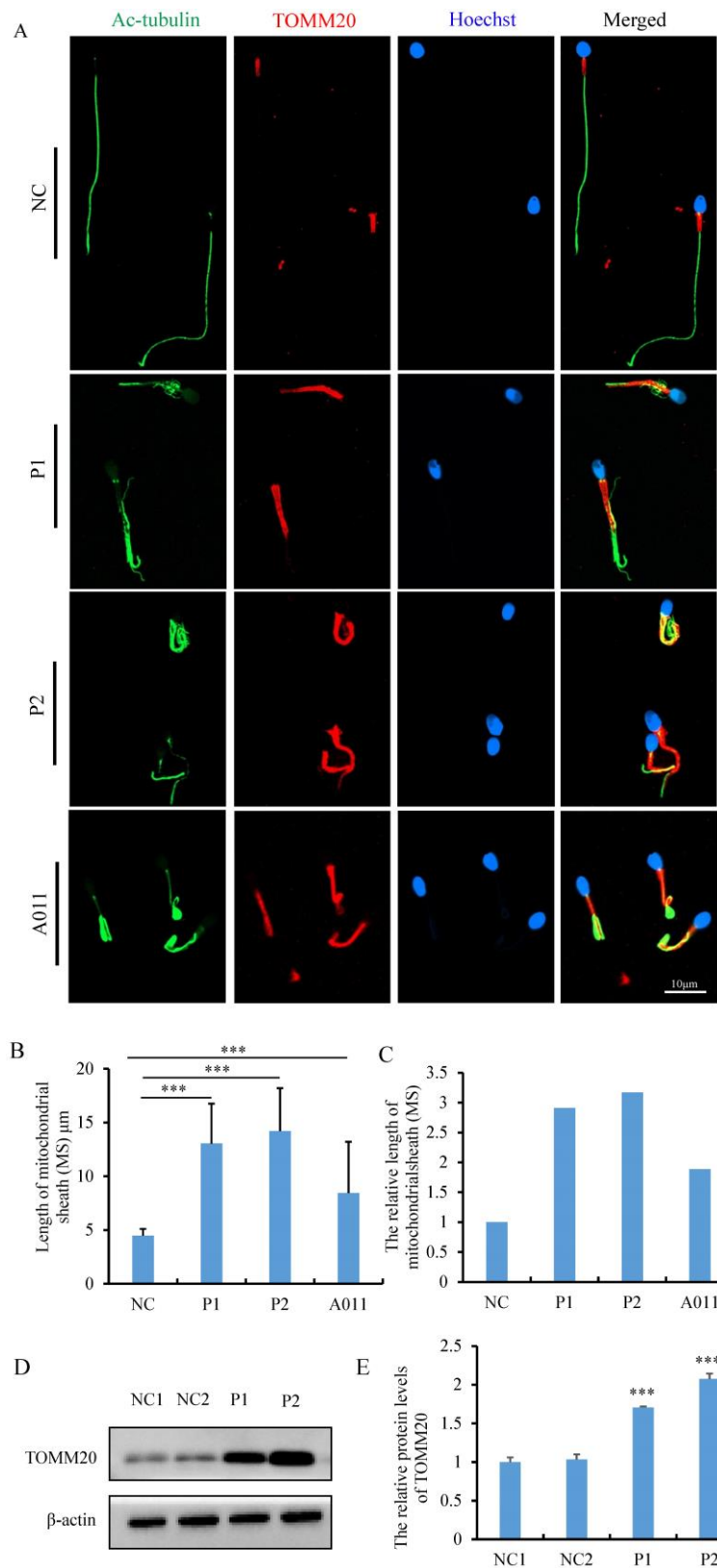


Figure 4. The measurement and analysis of MS length and levels of TOMM20 in sperm from controls and *FSIP2* patients. **(A)** The immunofluorescence staining analysis of TOMM20 in control subjects and *FSIP2* patients. Anti-TOMM20 (red) marked the sperm MS. Anti-ac-tubulin (green) marked the sperm flagella. The nuclei of spermatozoa were Hoechst-labeled (blue). Scale bars: 10 μm. **(B-C)** Quantification of the length of MS in sperm from controls and *FSIP2* patients according to the TOMM20 signals. The measurements were performed using the LSM 800 confocal microscope image processing and quantification tools. 115, 75, 111 and 113 sperm from normal control, P1, P2 and A011 were used to estimate the length of the MS. The average length of mitochondrial sheath was 4.47±0.63 μm in sperm from normal controls, while, which were 13.04±3.71 μm (P1), 14.20±3.99 μm (P2) and 8.43 ±4.77 μm (A011) of sperm from subjects harboring *FSIP2* variants, 2-3 times of that in control sperm. **(D-E)** The levels of TOMM20 in sperm cells from normal individual and *FSIP2*-deficient subjects analyzed by western blot. The abundances of TOMM20 were increased nearly two times in men harboring *FSIP2* variants when compared with those of the control individual. β-actin was used as internal reference.

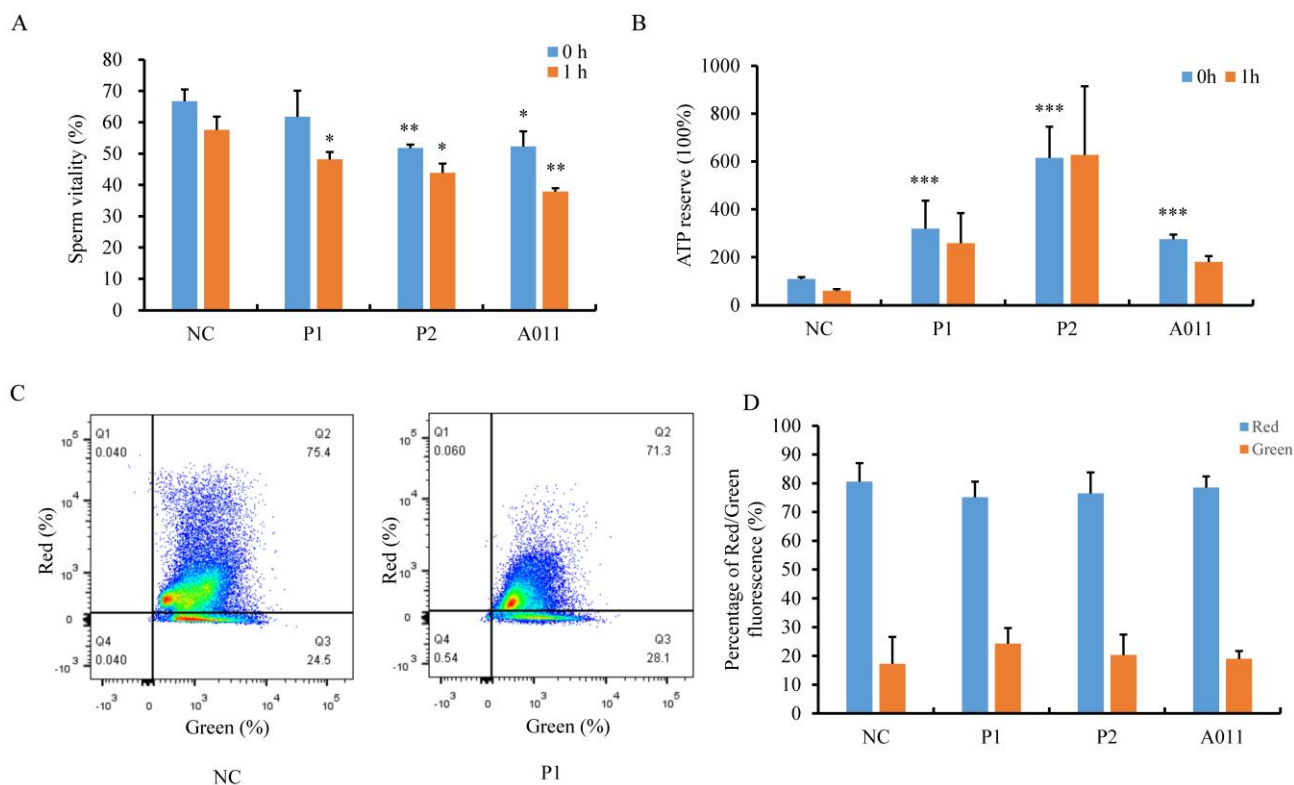


Figure 5. The assessment of sperm mitochondrial function in normal individual and *FSIP2*-deficient subjects. (A) The percentage of live spermatozoa was calculated in normal controls and patients. The liquefied spermatozoa were stained with eosin immediately ($t=0$) or 1 hour later ($t=1$), the total number and proportion of stained and unstained spermatozoa were calculated. Student t -test; $n=3$, n presents the number of repetitions, * $P<0.05$, ** $P<0.01$. **(B)** ATP reserve and consumption of sperm from control and patients. ATP content was measured by a luciferase method immediately after liquefaction ($t=0$) and after 1 hour of incubation at 37°C in 5% CO_2 atmosphere ($t=1$). **(C and D)** Spermatozoa mitochondrial membrane potential (MMP) was examined by flow cytometry acquisition for JC-1-stained (a marker of MMP) and statistically analyzed. Red fluorescence presented the high MMP and green fluorescence indicated the low MMP.

Next, we attempted to determine the function of the lengthened MS. First, we examined sperm viability by staining liquefied spermatozoa with eosin immediately ($t=0$) or 1 hour later ($t=1$). We observed that percentages of live spermatozoa were decreased in P2 and A011, and more dead spermatozoa were found after 1h in individuals carrying *FSIP2* variants compared with normal controls (Fig. 5A). We then measured ATP content and ATP consumption in sperm from fertile controls and patients. Unexpectedly, spermatozoa from individuals with *FSIP2* variants contained far more ATP than normal controls. After incubation at 37°C for 1h, the ATP levels of normal sperm was decreased by more than 50%, whereas, ATP consumptions were considerably lower in sperm from *FSIP2*-deficient patients (P1 and P2) than normal controls, and the ATP consumption was not affected severely in A011 (Fig. 5B). Moreover, we also analyzed the mitochondrial membrane potential (MMP) through FACS using JC-1 staining of spermatozoa from controls and *FSIP2*-deficient patients. As shown in Fig. 5C and D, the MMPs were reduced slightly in sperm from *FSIP2*-deficient patients compared with control. These findings revealed that deficiency of *FSIP2* resulted in mitochondrial dysfunction in human sperm.

The mitochondrial sheath in the sperm mid-piece is the final piece of sperm flagella that is formed during spermatogenesis. The length of mid-piece and the number of gyres are strictly regulated. The mechanisms that drive such processes during spermatogenesis have received little attention. To study the potential factors affecting spermatozoa MS length in individuals carrying the *FSIP2* variants, we used immunofluorescence to analyze the presence and localization of the annulus protein SEPT4, a critical component of the annulus ring that separates the middle and principal pieces. Using fluorescence microscopy, we detected SEPT4 as a dot located at the end of spermatozoa MS in healthy controls (Fig. 6A I). However, the presence and localization of SEPT4 signals were disrupted in most of sperms from *FSIP2* deficient individuals (P1 and P2) including presentation on the MS (0.9% & 0.4%, Fig. 6A II), the proximal region of the MS (0.7% & 0.6%, Fig. 6A III), and the distal region of the MS (37.7% & 29.8%, Fig. 6A IV-V and B). More than half of the analyzed sperms, SEPT4 signals were missing from the sperm flagella (60.7% & 69.2%, Fig. 6A VI and B), which were in accordance with the result that SEPT4 levels were lower in individuals with *FSIP2* deficiency (Fig. 6C). To determine whether the dislocation or absence of

annulus ring was the direct cause of the lengthened MS, we detected the length of MS in men harboring *SEPT4* variants. As shown in Fig. S2A, the *SEPT4* staining signals were absent in men harboring *SEPT4* variants, while the lengthened MS were not observed (Fig. S2B). Therefore, our results indicated that the lengthening of spermatozoa MS in individuals with *FSIP2* deficiency may be due to dislocation or absence of the FS, not the annulus ring.

Individuals carrying *FSIP2* variants lack AKAP4 protein and have altered distribution of axonemal components and IFT-B complexes

To explore the ultrastructural defects observed in the principal piece, we measured the localizations and levels of different substructures of the FS and axoneme component proteins, including SPAG6 (a component of the CP complex), AKAP4 (a protein that localizes to the FS), and DNAI2 (dynein axonemal intermediate chain 2, a component of outer dynein arm (ODA)). We found that SPAG6, AKAP4, and DNAI2 signals were normally localized along the sperm flagella in control sperm but were almost absent in sperms of men carrying *FSIP2* variants (Fig. 7A, B, and D), which were confirmed by WB assays (Fig. 7D). These findings suggested that the CP component, FS, and outer dynein arm (ODA) are affected by variants in *FSIP2*.

The IFT is a highly conserved bidirectional cargo delivery system that transports cilia/flagella-associated proteins along axonemal MTs to assemble and maintain cilia/sperm flagella. IFT complexes consist of at least 22 highly conserved proteins that are divided into two subcomplexes: IFT-A (minus-end-directed transport) and IFT-B (plus-end-directed transport) [27]. To determine the effect of *FSIP2* variants on the assembly of sperm flagellar axonemal protein complexes, the location and expression of the IFT-B subcomplex components IFT88, IFT74, and IFT20 were examined. IFT88, IFT74, and IFT20 staining signals were dislocated in P1 including concentrated at the mid-piece and distributed discontinuous along the flagella, and were almost absent in P2 (Fig. 8A, B and C). Western blots analysis in sperm lysates revealed that the levels of IFT88, IFT74 and IFT20 proteins in P1 were comparable with those in control and reduced significantly in P2 (Fig. 8D). These results may be related to the formation of truncated protein of *FSIP2*, which may affect the normal transport of IFTs. Collectively, our experimental observations indicate that *FSIP2* is required for the normal assembly of the axoneme for the normal transport of flagella-associated proteins to the assembly site.

Successful impregnation following intracytoplasmic sperm injection (ICSI) treatment of individuals carrying *FSIP2* variants

Three partners of men carrying *FSIP2* variants were unable to conceive spontaneously without contraception for more than one year. Majority of studies to date have demonstrated that ICSI treatment is an effective way of overcoming the physical limitations experienced by most individuals with asthenoteratozoospermia. The partner of study participant P1 had a normal basal endocrine assessment and a regular menstrual cycle. A total of 29 oocytes were retrieved following treatment with a gonadotropin-releasing hormone (GnRH) agonist. Of these, 24 metaphase II (MII) oocytes were microinjected, and 19 were successfully fertilized. Seven blastocysts were generated on the 5th day and frozen for 6 months to prevent development of ovarian hyperstimulation syndrome. P1's partner became pregnant after the second frozen embryo transfer (Table 3).

Similarly, following treatment with an antagonist regimen, twelve oocytes were retrieved from the partner of study participant P2. Eleven MII oocytes were successfully microinjected, and five were fertilized and cleaved. Three high-quality blastocysts were subsequently frozen. Six months later, two blastocysts were transferred after thawing, resulting in pregnancy and detection of a single fetal heartbeat via ultrasound, and gave birth to a healthy child (Table 3). Unfortunately, information of the assisted reproductive cycle of the third couple was lost and the semen specimen could not be obtained for the molecular experiments above. Retrospect to the subject with the *FSIP2* variant (A011) we reported in 2018[32], we found that the partner of A011 had a normal basal endocrine assessment and a regular menstrual cycle. Following treatment with an antagonist regimen, seventeen oocytes were retrieved and fourteen MII oocytes were successfully microinjected. Finally, eleven oocytes were fertilized and cleaved, and seven high-quality blastocysts were subsequently frozen. One blastocyst was transferred and a healthy baby was born. Overall, our study shows that male infertility caused by *FSIP2* variants can be rescued by ICSI treatment. Successful outcomes in these three couples provide guidance on clinical treatment options for patients with MMAF who carry *FSIP2* variations and similar variants and provide evidence of successfully applying assisted reproduction techniques to help patients with idiopathic asthenoteratozoospermia conceive.

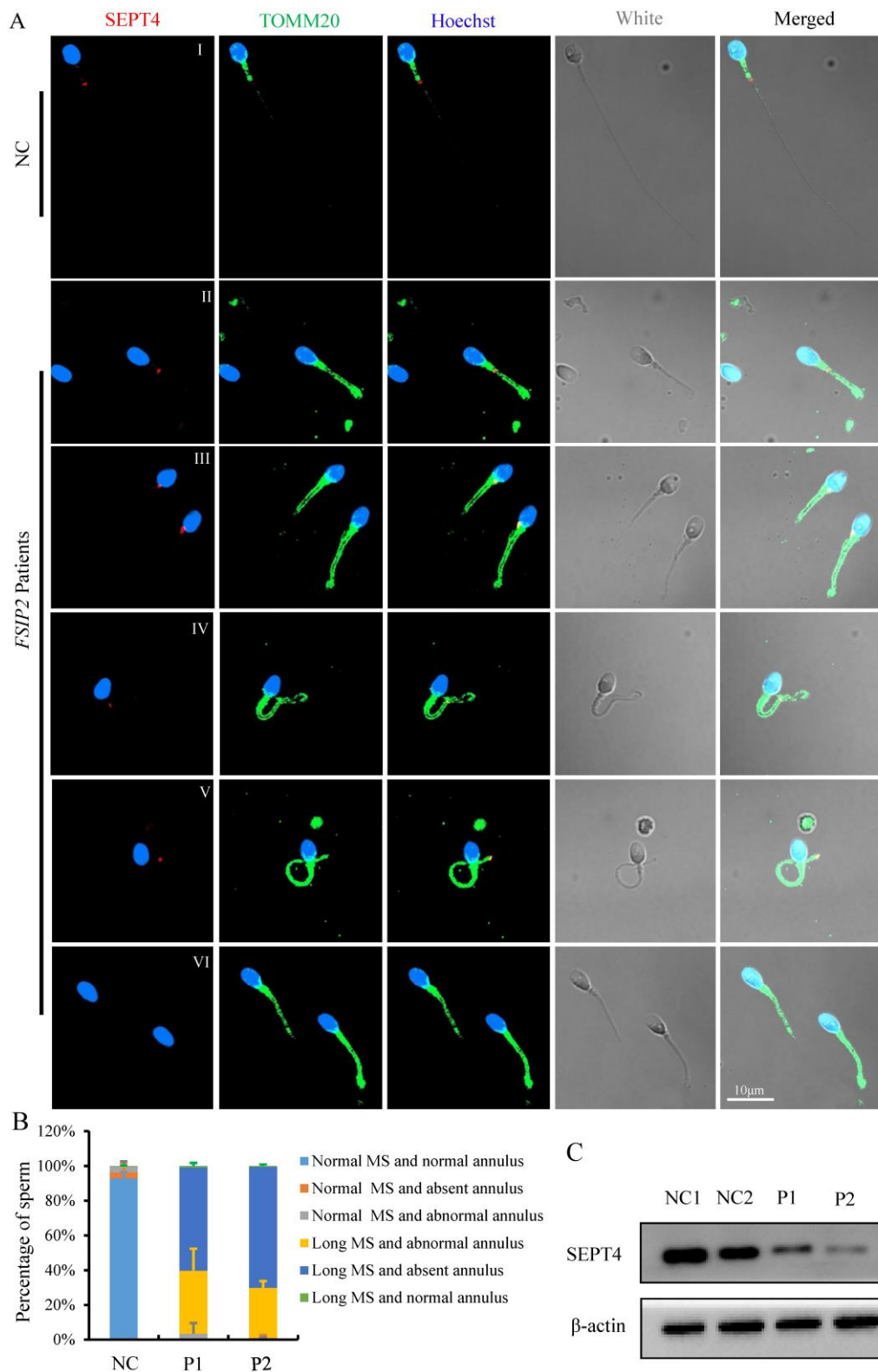


Figure 6. The immunofluorescence staining analysis of the presence and localization of sperm annulus ring in normal individual and *FSIP2*-deficient subjects. (A) The presence and localization of SEPT4 and TOMM20 staining signals in normal individual and *FSIP2*-deficient subjects. In normal sperm, the SEPT4 staining signal was located at the end of the MS, while the presence and localization of SEPT4 were disrupted in most of the analyzed sperm from *FSIP2* deficiency subjects, including presenting on the MS, proximal region of MS, distal region of MS and absence of SEPT4 on the sperm flagella, which accompanied by MS elongation. Anti-TOMM20 (green) marked the sperm MS. Anti-SEPT4 (red) marked sperm annulus ring. The nuclei of spermatozoa were Hoechst-labeled (blue). Scale bars: 10µm. **(B)** Quantification of different categories of sperm annulus ring and MS defects. Immunofluorescence (IF) analysis was performed using sperm cells from three fertile controls and patients carrying *FSIP2* variants (patient 1 (P1) and patient 2 (P2)). At least three semen samples from each patient were collected over 3 months through masturbation after 3-7 days of sexual abstinence. More than 200 spermatozoa from each sample were analyzed. The average sperm numbers for quantification in the control subjects and men harboring *FSIP2* variants (P1 and P2) were 240, 222 and 228, respectively. Sperm annulus ring and MS defects were classified into five categories: normal MS and absent annulus (0 & 0.8%), normal MS and abnormal annulus (0 & 0.2%), long MS and abnormal annulus (38.4% & 30.4%, III-V), long MS and absent annulus (60.7% & 69.2%, VI) and long MS and normal annulus (0.9% & 0.4%, II). **(C)** The levels of SEPT4 in sperm cells from normal individual and *FSIP2*-deficient subjects analyzed by western blot. The levels of SEPT4 were reduced in men harboring *FSIP2* variants. β-actin was used as internal reference.

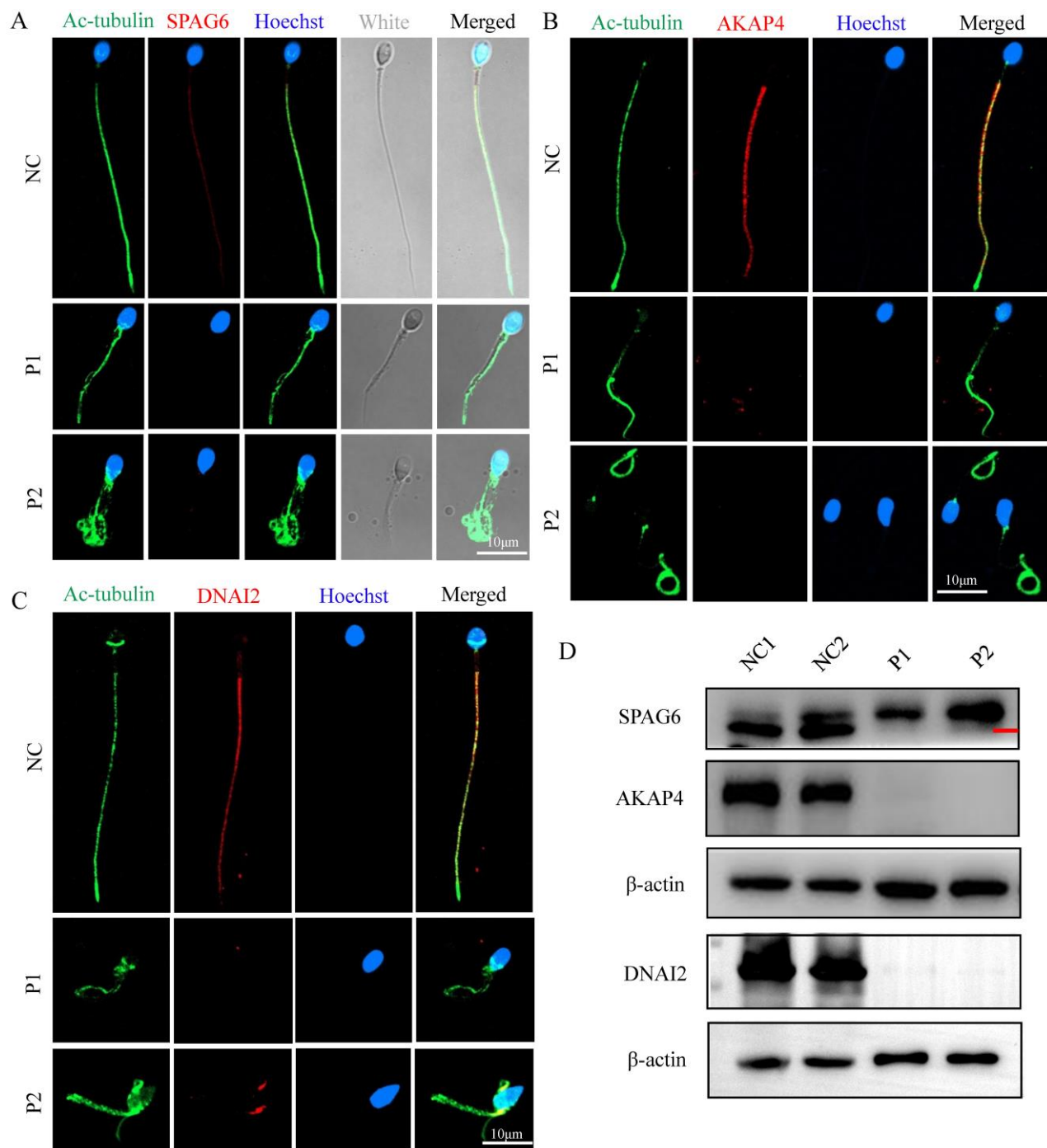


Figure 7. The localization and levels of flagella associated proteins in *FSIP2* patients and controls. (A-C) Immunofluorescence assays of flagella associated proteins including SPAG6 (a component of the CP complex), AKAP4 (a protein described to localize to the fibrous sheath), and DNAI2 (Dynein Axonemal Intermediate Chain 2) in *FSIP2* patients and controls. Anti-SPAG6 (red in A), anti- AKAP4 (red in B) and Anti- DNAI2 (red in C) normally localized along the sperm flagella in the control sperm. Signals of SPAG6, AKAP4 and DNAI2 were almost absent in sperm obtained from men harboring *FSIP2* variants. Anti-ac-tubulin (green) marked the sperm flagella. The nuclei of spermatozoa were Hoechst-labeled (blue). Scale bars: 10 μ m. (D) WB assays analysis the levels of SPAG6, AKAP4, and DNAI2 in sperm obtained from men harboring *FSIP2* variants and normal control. The results of WB assays were accordance with those of immunofluorescence assays described above.

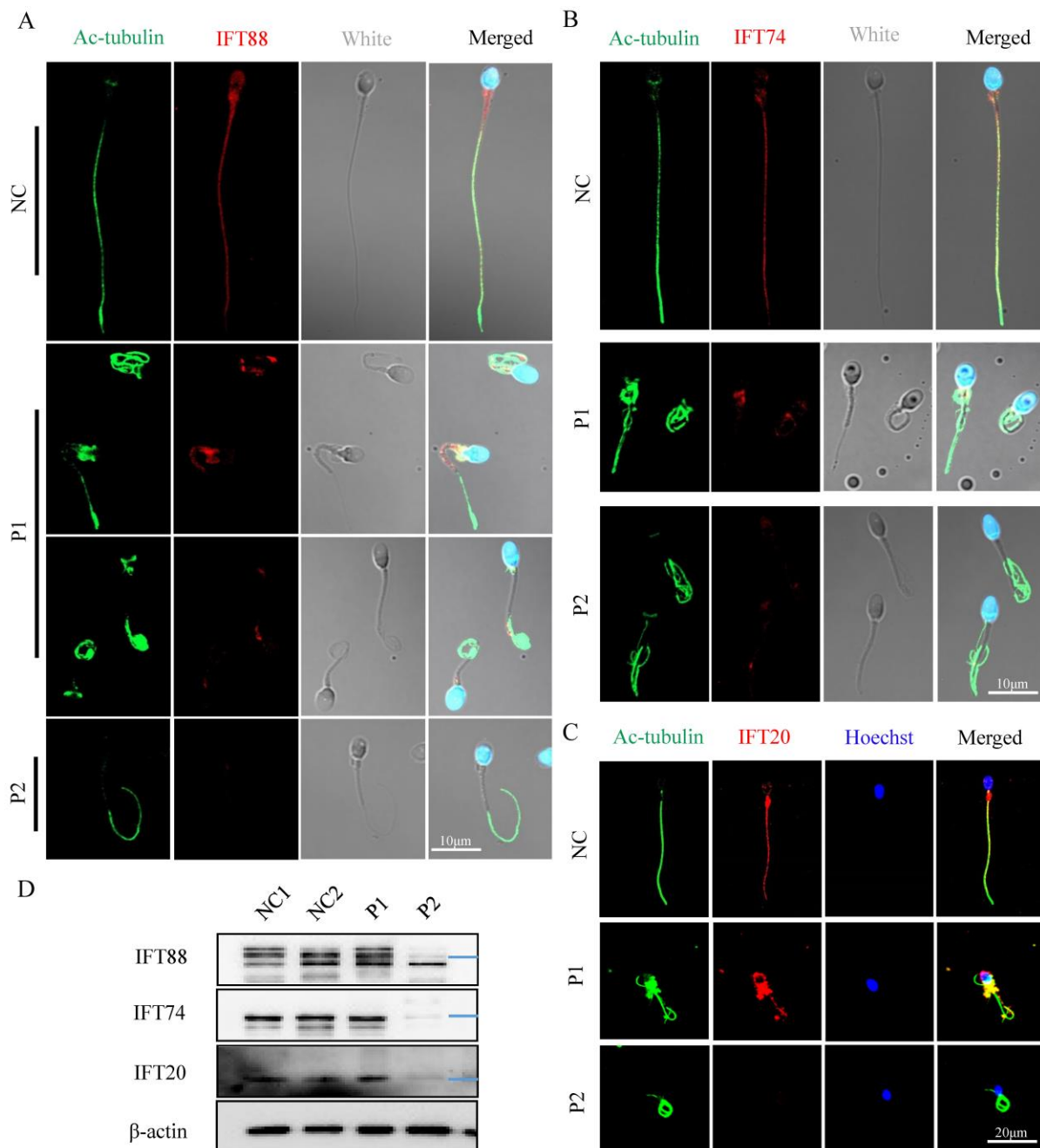


Figure 8. The localization and levels of IFT-B related proteins (IFT88, IFT74, IFT20) staining signals in normal individual and *FSIP2*-deficient subjects. **(A)** Immunofluorescence staining assays were performed on the spermatozoa using anti-IFT88 (red) and anti- α -tubulin (green) antibodies. DNA was counterstained with Hoechst as a nuclear marker. Scale bars: 10 μ m. **(B)** Immunofluorescence staining assays were performed on the spermatozoa using anti-IFT74 (red) and anti- α -tubulin (green) antibodies. DNA was counterstained with Hoechst as a nuclear marker. Scale bars: 10 μ m. **(C)** Immunofluorescence staining assays were performed on the spermatozoa using anti-IFT20 (red) and anti- α -tubulin (green) antibodies. DNA was counterstained with Hoechst as a nuclear marker. Scale bars: 20 μ m. **(D)** The levels of IFT88, IFT74 and IFT20 in sperm of normal individual and *FSIP2* deficient subjects were detected by WB assays. β -actin was used as internal reference.

Discussion

In this study, we identified novel compound heterozygous *FSIP2* variants in three unrelated individuals in a cohort of 105 patients with asthenoteratozoospermia. *FSIP2* has previously been associated with FS formation. Despite recent studies showing an association between the *FSIP2* truncated variant and the MMAF phenotype [31-33, 42, 53],

many questions still remain. In this study, TEM analyses of sperm from individuals carrying *FSIP2* variants revealed severe dysplasia of FS, including missing FS and failure to form longitudinal FS columns (3rd and 8th), leading to extremely disorganized and hypertrophic FS. These FS defects have previously been reported in patients carrying *FSIP2* and *AKAP4* variants and are termed DFS. These FS defects do not appear to be present in sperm cells of individuals with MMAF who have variants in the

axonemal genes *DNAH1*, *SPAG6*, and *TTC21A* [12, 22, 54]. Sperms of individuals carrying *FSIP2* variants also displayed some axonemal anomalies, including the absence of CP and the disorganization of DMT, and dynein arms, similar to those of individuals with MMAF who carry other gene variants. While the presence of multiple flagellar axonemes surrounding the mid-piece wrapped in excess residual cytoplasm had not been analyzed previously in subjects with MMAF harboring axonemal related gene variants. We also observed that staining signals associated with IFT-B-related proteins: IFT88, IFT74, and IFT20, were dislocated or absent in individuals with *FSIP2* deficiency. Protein-protein interaction network analysis by STRING showed that *FSIP2* may be highly connected with *FSIP1* and *CFAP69*. The protein level of IFT20 was downregulated significantly in the *Fsip1*^{-/-} mice testis and *FSIP1* interacted with IFT20 involving sperm flagellum assembly [42]. Additionally, *SPEF2* possible had the role in protein through the manchette towards the sperm tail interacting with IFT20 and *CFAP69* [55, 56]. Thus, we can presume that *FSIP2* is not only a structural protein of the FS but can also serve as an intra-flagellar transporter, binding to IFT20, one component of IFT-B complexes. This suggests that *FSIP2* plays an important role in maintaining the structure and function of sperm flagellum.

Table 3. The clinical outcomes of *FSIP2* mutated subjects ICSI

	<i>FSIP2</i> Mutated Subjects			
	P1	P2	P3	A011
No. of couples	4			
Subjects	P1	P2	P3	A011
Male age (year)	30	27	29	28
Female age (year)	29	27	28	27
No. of ICSI cycles	1	1	1	
No. of oocytes retrieved	29	12	/	19
No. of oocytes injected	24	11	/	14
Fertilization rate (%)	79.2 (19/24)	45.5(5/11)	/	78.6 (11/14)
Cleavage rate (%)	100(19/19)	100(5/5)	/	100 (11/11)
8-Cell formation rate (%)	63.2(12/19)	80(4/5)	/	72.7 (8/11)
Blastocyst formation rate (%)	36.8(7/19)	60(3/5)	/	72.7 (8/11)
High quality blastocyst rate (%)	15.8(3/19)	60(3/5)	/	63.6 (7/11)
No. of transfer cycles	2	1	/	1
Number of embryos transferred per cycle	2	1	/	1
Implantation rate (%)	25(1/4)	100(1/1)	/	100(1/1)
Clinical pregnancy rate per transfer cycle (%)	50(1/2)	100(1/1)	/	100(1/1)
Miscarriage rate (%)	50(1/2)	0	/	0
Live birth	Yes	Yes	/	Yes

In addition to the severe abnormalities of the axoneme and FS structures described above, sperm from patients carrying *FSIP2* variants also had elongated MS in the sperm mid-piece and the elevated levels of MS protein TOMM20. Mitochondrial ATP content also increased consistently, however, mitochondrial utilization decreased,

suggesting that ATP producing systems were not affected. Previous study found that mitochondrial DNAs (mtDNAs) content were increased during meiosis and early spermatogenesis in the mouse testis and 8-10-fold of mtDNAs were eliminated at the time of differentiation of the round spermatids into elongated spermatids [35, 57, 58]. *FSIP2* was transcribed in late spermatocyte development. We postulate that *FSIP2* may associate with the process of mitochondria multiplication during meiosis and early spermatogenesis, or the process of the retention of mitochondria during differentiation of the round spermatids into elongated spermatids, little is known about it, which should be further study in the *Fsip2* KO mice. The reduced mitochondrial consumption may be resulted from the serious damaged flagellar structure of spermatozoa, inducing sperm more likely to immotile or to die after collection, and a partial decrease in mitochondrial membrane potential. The dynein, major ATP-consuming motor protein, may be disrupted due to *FSIP2* deficiency during sperm flagellar assembly, which may also probably responsible for the low ATP consumption.

Analysis of spermatogenesis in rats revealed that longitudinal FS columns begin to appear around the distal end of the axoneme immediately after axoneme initiation, and then extend 'backwards' as the axoneme extends. Following the movement of the annulus ring during spermatogenesis, the proximal region of ODFs and axoneme is exposed, allowing the mitochondria to assemble and generate the mid-piece, supplying energy that maintains sperm motility. Both mitochondrial length and gyre numbers are strictly regulated [27]. However, the mechanisms underlying mitochondrial keeping or removing during spermatogenesis remain unclear. The annulus ring is located between the middle and principal pieces and is an important physical barrier to the intra-flagellar transport of spermatozoa [59-62]. The annulus is often missing in sperm with primarily MS defects, not in MMAF. In this study, the lengthened MSs were thought to be the results of the missing annulus ring and the dislocation or absence of annulus-associated protein *SEPT4* between the mid and principal pieces. However, we found that the lengthened MSs were not existing in sperm from individuals carrying *SEPT4* variants (Fig.S2B), indicating that the termination of MS extension may be determined by the *FSIP2* protein, rather than the position of the annulus ring. This hypothesis was confirmed by that *Cfap157*-deficient sperm presented with axonemal loops, clustered mitochondria in the midpiece regions, abnormal distribution of fibrous sheath in the principle pieces and normal annulus rings between them [37]. However, current data are far from

definitive, and mechanism studies are required to further confirm the hypothesis.

Although knockout of *Cfap157*, *Armc12*, *Tbc1d21*, *Mff*, *Gk2*, *Sept4*, *Fsip1* and other genes in mouse had been reported to cause various malformation in sperm MS assembly, including mitochondrial aggregation, loose assembly, and short MS [37-41, 60]. In humans, in addition to the specific flagellum defects presented in the MMAF phenotype, variations in *CFAP65* (MIM: 614270), *CFAP58* (MIM: 619129), *EIF4G1* (MIM: 600495), and *DNHD1* (MIM: 617277) also induced sperm MS abnormalities [19, 46-48]. However, no variations had been reported to cause the lengthened MS sperm in human, the similar phenotype as in *FSIP2*. Different from *AKAP4*, *AKAP3*, and *FSIP1*, *FSIP2* was transcribed in late spermatocyte development [30]. Deficiencies of *FSIP2* were associated with DFS, MMAF and globozoospermia [31-33, 42]. Recurrent *FSIP2* amplification had been linked to testicular germ cell tumor [63], and *FSIP2* was also reported as a novel potential candidate gene for nonobstructive azoospermia [64]. Here, we found that biallelic variants of *FSIP2* were not only associated with DFS, MMAF described previously, but also related to the multiple axoneme, the lengthened MS and lower mitochondrial ATP utilization. These findings indicated that *FSIP2* might play key roles during spermatogenesis. However, the mechanisms underlying *FSIP2* involving in mitochondrial keeping or removing, organization, and termination of MS extension during spermatogenesis remain unclear, which need to be further study.

In our study, the frameshift mutations M1 in P1, M3 and M4 in P2, M5 in P3 created a premature termination codon (PTC) downstream. The stop-gain mutation M2 in P2 also introduced a PTC at the place of mutation. 'Nonsense' and frameshift mutations are associated with low mRNA induced by nonsense-mediated mRNA decay (NMD) [65]. The missense variant M6 (c.9043G>A (p.E3015K)) in P3 at the last part of exon 16 of *FSIP2* may affect the pre-mRNA splicing process lead to PTC and result in NMD [66, 67]. Thus, the expression levels of *FSIP2* mRNA were reduced significantly in the three patients.

Previous reports identified seven homozygous and two compound heterozygous variants of *FSIP2* in individuals with MMAF. ICSI treatment outcomes in individuals carrying seven homozygous *FSIP2* variants were not included. The partner of one of the two patients carrying compound heterozygous *FSIP2* variants did not achieve pregnancy, whereas the other achieved good clinical outcomes after assisted reproductive therapy using ICSI. In this study, two of three men carrying compound heterozygous *FSIP2* variants and one subject harboring homozygous

FSIP2 variant we reported previously achieved successful ICSI outcomes (outcome information for the third patient was lost). Our findings can be used during genetic counseling of individuals with MMAF and asthenoteratozoospermia who carry *FSIP2* variants, prior to commencing ICSI treatment.

Although the findings of this study are interesting, the present study has some limitations, especially there was no *Fsip2* knockout (KO) mice model to detect the effect of *Fsip2* gene on the process of spermatogenesis. Therefore, identification of a larger number of individuals carrying *FSIP2* variants and generation of *Fsip2* KO mice are needed to elucidate the detail molecular mechanism of *Fsip2* gene influence on MS assembly, MS function and flagellum formation during spermatogenesis.

Conclusion

Our experimental observations of humans carrying *FSIP2* variants indicate that *FSIP2* deficiency not only leads to severe dysplasia of the FS but also induces total destabilization of the axoneme, an MMAF phenotype caused by the axonemal gene. Extremely disorganized or missing FS led to a loss of the annulus and an elongated "super-length" MS. Moreover, successful pregnancy outcomes could be achieved following ICSI treatment of spermatozoa from men carrying *FSIP2* variants. Overall, our findings expand the variants spectrum of *FSIP2* and improve our understanding of the new phenotype of spermatozoa in men carrying *FSIP2* variants.

Abbreviations

MMAF: multiple morphological abnormalities of the sperm flagella; WES: whole-exome sequencing; H&E: Hematoxylin-Eosin; SEM: Scanning electron microscopy; TEM: transmission electron microscopy; RT-qPCR: quantitative real-time polymerase chain reaction; MS: mitochondrial sheath; FS: fibrous sheath; CP: central pair; DMT: doublets of microtubules; ODF: outer dense fibers; ERC: excess residual cytoplasm; IF: immunofluorescence; WB: western blot.

Supplementary Material

Supplementary figures and tables.
<https://www.ijbs.com/v19p0393s1.pdf>

Acknowledgements

We would like to thank all individuals who participated in this study. We thank the Center for Scientific Research of Anhui Medical University for assistance with SEM and TEM work, and we would be grateful to Zhenhai Tang and Haijian Cai for their help of taking images.

Funding

This work was supported by the National Key R&D Program of China (2021YFC2700901), National Natural Science Foundation of China (82071705, 81971441, 82101681, and 82171607), the University Outstanding Young Talents Support Program (gxyq2021174), Non-profit Central Research Institute Fund of Chinese Academy of Medical Sciences (2019PT310002), Research Fund of Anhui Institute of Translational Medicine (ZHYX2020A001), the University Synergy Innovation Program of Anhui Province (GXXT-2021-071) and Scientific Research (TP202002) from Anhui Medical University.

Author contributions

M.L., D.T., H.Y., H.G., and Y.Z. contributed equally to this work. Y.C., F.Z. and X.H. conceived and designed the experiments. H.G., Q.T., C.X., Z.D., J.Z., H.W. and F.F. collected the clinical samples and analyzed sperm. Y.G., D.T., C.L., K.L. and C.L. organized the medical records and analyzed the whole exome data. M.L., D.T., H.Y., Z.S., S.G., G.W., Y.Z. and K.W. performed the experiments and analyzed the experiments data. Y.C., F.Z., X.H. and M.L. drafted the article and revised the manuscript. R.G., R.H., Y.X., P.Z. and Z.W. provided important guidance for the study. All authors approved the final manuscript.

Competing Interests

The authors have declared that no competing interest exists.

References

- Krausz C, Riera-Escamilla A. Genetics of male infertility. *Nature reviews Urology*. 2018; 15: 369-84.
- Krausz C, Riera-Escamilla A, Moreno-Mendoza D, Holleman K, Cioppi F, Algaba F, et al. Genetic dissection of spermatogenic arrest through exome analysis: clinical implications for the management of azoospermic men. *Genet Med*. 2020; 22: 1956-66.
- Yan J, Liu C, Zhao H, Wang C, Yao H, Lu Q, et al. A cross-sectional study on the correlation between cytokines in a pelvic environment and tubal factor infertility. *BMC Pregnancy Childbirth*. 2020; 20: 644.
- Stephen EH, Chandra A. Declining estimates of infertility in the United States: 1982-2002. *Fertil Steril*. 2006; 86: 516-23.
- Colpi GM, Francavilla S, Haidl G, Link K, Behre HM, Goulis DG, et al. European Academy of Andrology guideline Management of oligo-astheno-teratozoospermia. *Andrology*. 2018; 6: 513-24.
- Inaba K. Sperm flagella: comparative and phylogenetic perspectives of protein components. *Mol Hum Reprod*. 2011; 17: 524-38.
- Inaba K. Molecular basis of sperm flagellar axonemes: structural and evolutionary aspects. *Ann N Y Acad Sci*. 2007; 1101: 506-26.
- Toure A, Martinez G, Kherraf ZE, Cazin C, Beurois J, Arnoult C, et al. The genetic architecture of morphological abnormalities of the sperm tail. *Hum Genet*. 2021; 140: 21-42.
- Wang WL, Tu CF, Tan YQ. Insight on multiple morphological abnormalities of sperm flagella in male infertility: what is new? *Asian J Androl*. 2020; 22: 236-45.
- Ray PF, Toure A, Metzler-Guillemain C, Mitchell MJ, Arnoult C, Coutton C. Genetic abnormalities leading to qualitative defects of sperm morphology or function. *Clin Genet*. 2017; 91: 217-32.
- Ross A, Christie S, Edmond P. Ultrastructural tail defects in the spermatozoa from two men attending a subfertility clinic. *J Reprod Fertil*. 1973; 32: 243-51.
- Ben Khelifa M, Coutton C, Zouari R, Karaouzene T, Rendu J, Bidart M, et al. Mutations in DNAH1, which encodes an inner arm heavy chain dynein, lead

to male infertility from multiple morphological abnormalities of the sperm flagella. *Am J Hum Genet*. 2014; 94: 95-104.

- Gao Y, Tian S, Sha Y, Zha X, Cheng H, Wang A, et al. Novel bi-allelic variants in DNAH2 cause severe asthenoteratozoospermia with multiple morphological abnormalities of the flagella. *Reprod Biomed Online*. 2021; 42: 963-72.
- Tu C, Nie H, Meng L, Yuan S, He W, Luo A, et al. Identification of DNAH6 mutations in infertile men with multiple morphological abnormalities of the sperm flagella. *Sci Rep*. 2019; 9: 15864.
- Liu C, Miyata H, Gao Y, Sha Y, Tang S, Xu Z, et al. Bi-allelic DNAH8 Variants Lead to Multiple Morphological Abnormalities of the Sperm Flagella and Primary Male Infertility. *Am J Hum Genet*. 2020; 107: 330-41.
- Li K, Wang G, Lv M, Wang J, Gao Y, Tang F, et al. Bi-allelic variants in DNAH10 cause asthenoteratozoospermia and male infertility. *J Assist Reprod Genet*. 2022; 39: 251-9.
- Zhang B, Ma H, Khan T, Ma A, Li T, Zhang H, et al. A DNAH17 missense variant causes flagella destabilization and asthenozoospermia. *J Exp Med*. 2020; 217.
- Tang S, Wang X, Li W, Yang X, Li Z, Liu W, et al. Biallelic Mutations in CFAP43 and CFAP44 Cause Male Infertility with Multiple Morphological Abnormalities of the Sperm Flagella. *Am J Hum Genet*. 2017; 100: 854-64.
- He X, Liu C, Yang X, Lv M, Ni X, Li Q, et al. Bi-allelic Loss-of-function Variants in CFAP58 Cause Flagellar Axoneme and Mitochondrial Sheath Defects and Asthenoteratozoospermia in Humans and Mice. *Am J Hum Genet*. 2020; 107: 514-26.
- Li W, Wu H, Li F, Tian S, Kherraf ZE, Zhang J, et al. Biallelic mutations in CFAP65 cause male infertility with multiple morphological abnormalities of the sperm flagella in humans and mice. *J Med Genet*. 2020; 57: 89-95.
- Liu C, Tu C, Wang L, Wu H, Houston BJ, Mastrososa FK, et al. Deleterious variants in X-linked CFAP47 induce asthenoteratozoospermia and primary male infertility. *Am J Hum Genet*. 2021; 108: 309-23.
- Liu W, He X, Yang S, Zouari R, Wang J, Wu H, et al. Bi-allelic Mutations in TTC21A Induce Asthenoteratozoospermia in Humans and Mice. *Am J Hum Genet*. 2019; 104: 738-48.
- Liu C, He X, Liu W, Yang S, Wang L, Li W, et al. Bi-allelic Mutations in TTC29 Cause Male Subfertility with Asthenoteratozoospermia in Humans and Mice. *Am J Hum Genet*. 2019; 105: 1168-81.
- He X, Li W, Wu H, Lv M, Liu W, Liu C, et al. Novel homozygous CFAP69 mutations in humans and mice cause severe asthenoteratozoospermia with multiple morphological abnormalities of the sperm flagella. *J Med Genet*. 2019; 56: 96-103.
- Lv M, Liu W, Chi W, Ni X, Wang J, Cheng H, et al. Homozygous mutations in DZIP1 can induce asthenoteratozoospermia with severe MMAF. *J Med Genet*. 2020; 57: 445-53.
- Sha YW, Xu X, Mei LB, Li P, Su ZY, He XQ, et al. A homozygous CEP135 mutation is associated with multiple morphological abnormalities of the sperm flagella (MMAF). *Gene*. 2017; 633: 48-53.
- Pleuger C, Lehti MS, Dunleavy JE, Fietz D, O'Bryan MK. Haploid male germ cells—the Grand Central Station of protein transport. *Hum Reprod Update*. 2020; 26: 474-500.
- Turner RM, Musse MP, Mandal A, Klotz K, Jayes FC, Herr JC, et al. Molecular genetic analysis of two human sperm fibrous sheath proteins, AKAP4 and AKAP3, in men with dysplasia of the fibrous sheath. *J Androl*. 2001; 22: 302-15.
- Zhang G, Li D, Tu C, Meng L, Tan Y, Ji Z, et al. Loss-of-function missense variant of AKAP4 induced male infertility through reduced interaction with QRICH2 during sperm flagella development. *Hum Mol Genet*. 2021; 31: 219-31.
- Brown PR, Miki K, Harper DB, Eddy EM. A-kinase anchoring protein 4 binding proteins in the fibrous sheath of the sperm flagellum. *Biol Reprod*. 2003; 68: 2241-8.
- Martinez G, Kherraf ZE, Zouari R, Fourati Ben Mustapha S, Saut A, Pernet-Gallay K, et al. Whole-exome sequencing identifies mutations in FSP12 as a recurrent cause of multiple morphological abnormalities of the sperm flagella. *Hum Reprod*. 2018; 33: 1973-84.
- Liu W, Wu H, Wang L, Yang X, Liu C, He X, et al. Homozygous loss-of-function mutations in FSP12 cause male infertility with asthenoteratozoospermia. *J Genet Genomics*. 2019; 46: 53-6.
- Liu M, Sun Y, Li Y, Sun J, Yang Y, Shen Y. Novel mutations in FSP12 lead to multiple morphological abnormalities of the sperm flagella and poor ICSI prognosis. *Gene*. 2021; 781: 145536.
- Yuan Y, Xu WQ, Chen ZY, Chen Y, Zhang L, Zheng L, et al. Successful outcomes of intracytoplasmic sperm injection-embryo transfer using ejaculated spermatozoa from two Chinese asthenoteratozoospermic brothers with a compound heterozygous FSP12 mutation. *Andrologia*. 2022; 54: e14351.
- Vertika S, Singh KK, Rajender S. Mitochondria, spermatogenesis, and male infertility - An update. *Mitochondrion*. 2020; 54: 26-40.
- Otani H, Tanaka O, Kasai K, Yoshioka T. Development of mitochondrial helical sheath in the middle piece of the mouse spermatid tail: regular dispositions and synchronized changes. *Anat Rec*. 1988; 222: 26-33.
- Weidemann M, Schuster-Gossler K, Stauber M, Wrede C, Hegermann J, Ott T, et al. CFAP157 is a murine downstream effector of FOXJ1 that is specifically required for flagellum morphogenesis and sperm motility. *Development*. 2016; 143: 4736-48.

38. Shimada K, Park S, Miyata H, Yu Z, Morohoshi A, Oura S, et al. ARMC12 regulates spatiotemporal mitochondrial dynamics during spermiogenesis and is required for male fertility. *Proc Natl Acad Sci U S A*. 2021; 118.
39. Chen Y, Chen X, Zhang H, Sha Y, Meng R, Shao T, et al. TBC1D21 is an essential factor for sperm mitochondrial sheath assembly and male fertility. *Biol Reprod*. 2022; 107: 619-34.
40. Varuzhanyan G, Chen H, Rojansky R, Ladinsky MS, McCaffery JM, Chan DC. Mitochondrial fission factor (Mff) is required for organization of the mitochondrial sheath in spermatids. *Biochim Biophys Acta Gen Subj*. 2021; 1865: 129845.
41. Shimada K, Kato H, Miyata H, Ikawa M. Glycerol kinase 2 is essential for proper arrangement of crescent-like mitochondria to form the mitochondrial sheath during mouse spermatogenesis. *J Reprod Dev*. 2019; 65: 155-62.
42. Gamallat Y, Fang X, Mai H, Liu X, Li H, Zhou P, et al. Bi-allelic mutation in *Fsp1* impairs acrosome vesicle formation and attenuates flagellogenesis in mice. *Redox Biol*. 2021; 43: 101969.
43. Mundy AJ, Ryder TA, Edmonds DK. Asthenozoospermia and the human sperm mid-piece. *Hum Reprod*. 1995; 10: 116-9.
44. Wilton LJ, Temple-Smith PD, de Kretser DM. Quantitative ultrastructural analysis of sperm tails reveals flagellar defects associated with persistent asthenozoospermia. *Hum Reprod*. 1992; 7: 510-6.
45. Pelliccione F, Micillo A, Cordeschi G, D'Angeli A, Necozone S, Gandini L, et al. Altered ultrastructure of mitochondrial membranes is strongly associated with unexplained asthenozoospermia. *Fertil Steril*. 2011; 95: 641-6.
46. Wang W, Tu C, Nie H, Meng L, Li Y, Yuan S, et al. Biallelic mutations in *CFAP65* lead to severe asthenoteratozoospermia due to acrosome hypoplasia and flagellum malformations. *J Med Genet*. 2019; 56: 750-7.
47. Tan C, Meng L, Lv M, He X, Sha Y, Tang D, et al. Bi-allelic variants in *DNHD1* cause flagellar axoneme defects and asthenoteratozoospermia in humans and mice. *Am J Hum Genet*. 2022; 109: 157-71.
48. Sha Y, Liu W, Huang X, Li Y, Ji Z, Mei L, et al. *EIF4G1* is a novel candidate gene associated with severe asthenozoospermia. *Mol Genet Genomic Med*. 2019; 7: e807.
49. Gao Y, Wu H, Xu Y, Shen Q, Xu C, Geng H, et al. Novel biallelic mutations in *SLC26A8* cause severe asthenozoospermia in humans owing to midpiece defects: Insights into a putative dominant genetic disease. *Hum Mutat*. 2021.
50. Cong J, Wang X, Amiri-Yekta A, Wang L, Kherraf ZE, Liu C, et al. Homozygous mutations in *CCDC34* cause male infertility with oligoasthenoteratozoospermia in humans and mice. *J Med Genet*. 2021.
51. Dr. Christina Wang M. WHO laboratory manual for the examination and processing of human semen. 2021.
52. Lv M, Liu C, Ma C, Yu H, Shao Z, Gao Y, et al. Homozygous mutation in *SLO3* leads to severe asthenoteratozoospermia due to acrosome hypoplasia and mitochondrial sheath malformations. *Reprod Biol Endocrinol*. 2022; 20: 5.
53. Yuan Y, Xu WQ, Chen ZY, Chen Y, Zhang L, Zheng L, et al. Successful outcomes of intracytoplasmic sperm injection-embryo transfer using ejaculated spermatozoa from two Chinese asthenoteratozoospermic brothers with a compound heterozygous *FSIP2* mutation. *Andrologia*. 2021: e14351.
54. Xu C, Tang D, Shao Z, Geng H, Gao Y, Li K, et al. Homozygous *SPAG6* variants can induce nonsyndromic asthenoteratozoospermia with severe MMAF. *Reprod Biol Endocrinol*. 2022; 20: 41.
55. Sironen A, Hansen J, Thomsen B, Andersson M, Vilkki J, Toppari J, et al. Expression of *SPEF2* during mouse spermatogenesis and identification of *IIFT20* as an interacting protein. *Biol Reprod*. 2010; 82: 580-90.
56. Lehti MS, Zhang FP, Kotaja N, Sironen A. *SPEF2* functions in microtubule-mediated transport in elongating spermatids to ensure proper male germ cell differentiation. *Development*. 2017; 144: 2683-93.
57. N B Hecht HL. Mitochondrial DNA Is Synthesized During Meiosis and Spermiogenesis. *Exp Cell Res*. 1984; 293-8.
58. Hecht NB, Liem H, Kleene KC, Distel RJ, Ho SM. Maternal inheritance of the mouse mitochondrial genome is not mediated by a loss or gross alteration of the paternal mitochondrial DNA or by methylation of the oocyte mitochondrial DNA. *Dev Biol*. 1984; 102: 452-61.
59. Schmidt K, Nichols BJ. Functional interdependence between septin and actin cytoskeleton. *BMC Cell Biol*. 2004; 5: 43.
60. Kissel H, Georgescu MM, Larisch S, Manova K, Hunnicutt GR, Steller H. The *Sept4* septin locus is required for sperm terminal differentiation in mice. *Dev Cell*. 2005; 8: 353-64.
61. Hosseinifar H, Shafipour M, Modarresi T, Azad M, Sadighi Gilani MA, Shahhosseini M, et al. Relationship between absence of annulus and asthenozoospermia in Iranian men. *J Assist Reprod Genet*. 2014; 31: 1681-5.
62. Ihara M, Kinoshita A, Yamada S, Tanaka H, Tanigaki A, Kitano A, et al. Cortical organization by the septin cytoskeleton is essential for structural and mechanical integrity of mammalian spermatozoa. *Dev Cell*. 2005; 8: 343-52.
63. Litchfield K, Summersgill B, Yost S, Sultana R, Labreche K, Dudakia D, et al. Whole-exome sequencing reveals the mutational spectrum of testicular germ cell tumours. *Nat Commun*. 2015; 6: 5973.
64. Malkcher A, Stokowy T, Berman A, Olszewska M, Jedrzejczak P, Sielski D, et al. Whole-genome sequencing identifies new candidate genes for nonobstructive azoospermia. *Andrology*. 2022.
65. Carrier L, Schlossarek S, Willis MS, Eschenhagen T. The ubiquitin-proteasome system and nonsense-mediated mRNA decay in hypertrophic cardiomyopathy. *Cardiovasc Res*. 2010; 85: 330-8.
66. Kato K, Ohno S, Sonoda K, Fukuyama M, Makiyama T, Ozawa T, et al. LMNA Missense Mutation Causes Nonsense-Mediated mRNA Decay and Severe Dilated Cardiomyopathy. *Circ Genom Precis Med*. 2020; 13: 435-43.
67. Fukuyama M, Ohno S, Wang Q, Shirayama T, Itoh H, Horie M. Nonsense-mediated mRNA decay due to a CACNA1C splicing mutation in a patient with Brugada syndrome. *Heart Rhythm*. 2014; 11: 629-34.